Comparison of Canadian Air Quality Forecast Models With Tropospheric Ozone Profile Measurements Above Mid-Latitude North America During the IONS/ICARTT Campaign: Evidence for Stratospheric Input

D.W. Tarasick[1], M.D. Moran[1], A.M. Thompson[2], T. Carey-Smith[1], Y. Rochon[1], V.S. Bouchet[3], W. Gong[1], P.A. Makar[1], C. Stroud[1], S. Ménard[3], L.-P. Crevier[3], S. Cousineau[3], J.A. Pudykiewicz[4], A. Kallaur[1], R. Moffet[3], R. Ménard[1], A. Robichaud[1], O.R. Cooper[5], S.J. Oltmans[6], J.C. Witte[7], G. Forbes[8], B.J. Johnson[6], J. Merrill[9], J.L. Moody[10], G. Morris[11], M.J. Newchurch[12], F.J. Schmidlin[13], and E. Joseph[14]

[1]Air Quality Research Division, Environment Canada, Downsview, ON, Canada M3H 5T4

[2]Department of Meteorology, 510 Walker Building, Pennsylvania State University, University Park, PA, USA 16802

[3]Air Quality Models Applications Group, Meteorological Service of Canada, Environment Canada, 2121 TransCanada Highway, Dorval, QC, Canada H9P 1J3

[4]Meteorology Research Division, Environment Canada, Dorval, QC, Canada H9P 1J3

[5]Cooperative Institute for Research in Environmental Sciences (CIRES), University of Colorado/NOAA Aeronomy Laboratory, 325 Broadway, Boulder CO, USA 80305

[6]NOAA Climate Monitoring and Diagnostics Laboratory, 325 Broadway, Boulder CO, USA 80305

[7]Science Systems and Applications, Inc., NASA Goddard Space Flight Center, Mail Code 613.3, Greenbelt, USA 20771

[8]Meteorological Service of Canada, Sable Island, PO Box 622, Halifax CRO Halifax, NS, Canada B3J 2R7

[9]Graduate School of Oceanography, University of Rhode Island, South Ferry Road, Narragansett, RI, USA 02882

[10]Department of Environmental Sciences, University of Virginia, Charlottesville, Virginia, USA

[11]Department of Physics & Astronomy, Valparaiso University, Valparaiso, IN, USA 46383

[12]Atmospheric Science Department, University of Alabama in Huntsville, 320 Sparkman Drive, Huntsville, AL, USA, 35805

[13]Code 972, NASA/GSFC/Wallops Flight Facility, Wallops Island, Virginia, USA 23337

[14]Department of Physics & Astronomy, Howard University, 2355 6th St., NW Washington, D.C., USA 20059

Abstract. From July 1 to August 15, 2004, Environment Canada, NASA, NOAA, and several US universities pooled resources to release daily balloon-borne ozonesondes at 12 sites across the eastern USA and Canada under the INTEX Ozonesonde Network Study 2004 (IONS-04), part of the ICARTT (International Consortium for Atmospheric Research on Transport and Transformation) field experiment. At the same time, a number of air quality forecast models were run daily as part of ICARTT to provide guidance for aircraft deployment and other operational decisions. In this paper, we compare IONS ozonesonde profiles with predicted ozone profiles from two of these forecast models, the Environment Canada CHRONOS and AURAMS models. We find that the models show considerable skill at predicting ozone in the planetary boundary layer and immediately above. Individual station biases are variable, but often small. Standard deviations of observation-forecast differences are large, however. Ozone variability in the models is somewhat higher than observed. Most strikingly, neither model is able to reproduce the typical profile of increasing mixing ratio with altitude. In either case, the discrepancy could be considerably reduced by adding a downward flux of ozone from above the model lid. Estimates of the magnitude of this flux are compared with estimates of stratosphere-troposphere exchange made by other means.

1. Introduction

Ozone plays a major role in the chemical and radiative balance of the troposphere, controlling the oxidizing capacity of the lower atmosphere and also acting as an important greenhouse gas. It is also a principal indicator of air quality (AQ), and ozone in association with particulate matter in the lower troposphere has implications for human health. The Canadian AQ forecast models CHRONOS (Canadian Hemispheric and Regional Ozone and NO_x System) and AURAMS (A Unified Regional Air-quality Modelling System) have been developed by Environment Canada (EC) in order to understand better the atmospheric processes governing air quality, to evaluate different possible AQ management options, and to provide public forecasts of air quality in the short (48-hour) term. Given these different applications, it is important to characterize model performance for a range of model chemical species, geographic locations, seasons, and heights. However, evaluation of model forecasts has been conducted to date primarily with surface measurements [e.g., *Sirois et al*., 1999; *Gong et al*., 2006].

During the ICARTT (International Consortium for Atmospheric Research on Transport and Transformation) field campaign (July 1 – August 15, 2004), EC, NASA, NOAA, and several U.S. universities pooled resources to release 275 ozonesondes from a dozen sites across the eastern USA and Canada under the IONS-04 (INTEX Ozonesonde Network Study 2004) program [see overview by *Thompson et al*., 2006]. At the same time, daily 48-h model runs were performed with CHRONOS and AURAMS during ICARTT. The model forecasts provided guidance for planning EC aircraft operations during the field campaign, and they were also submitted to NOAA as part of an evaluation of real-time AQ forecasts that was a subcomponent of ICARTT [*McKeen et al*., 2005]. The IONS measurements present an

unprecedented opportunity to compare vertical ozone distributions predicted by the two AQ models with time- and space-resolved ozonesonde data during the most photochemically active part of the year.

The IONS data set and the two AQ models and their run configurations are described in the next section. One additional CHRONOS run and two additional AURAMS runs conducted since the IONS study period are also included in order to examine particular features of the models. A set of comparisons of ozonesonde profiles and model-predicted profiles for the five model versions are presented in Section 3, followed by a discussion of the results and conclusions in Sections 4 and 5, respectively.

2. Data Set and Model Simulations

2.1 Ozonesonde profiles

During the IONS-04 campaign ozonesonde profile data was collected at the 12 sites described in Table 1. Site locations are also indicated in Figure 1. All sites flew electrochemical concentration cell (ECC) ozonesondes, either the 2Z model manufactured by EnSci Corp. or the 6A model manufactured by Science Pump, with some variation in concentration of the KI sensing solution and of its phosphate buffer. The maximum variation in tropospheric response resulting from these differences is likely of the order of 2-3% [*Smit et al.,* 2006] and so is of minor importance for the purposes of this comparison. ECC ozonesondes have a precision of about 5% and an absolute accuracy of about 10% in the troposphere [*World Climate Research Programme*, 1998; *Smit et al.,* 2006; *Kerr et al*, 1994]. Data are typically reported at 10-second intervals, and the balloon ascent rate is about 4-5 m s^{-1}. As the ozone sensor has a response with an exponential time constant of about 20 s, this rapid ascent rate can lead to some distortion of

the profile that may be important to consider here for sharp vertical transitions in the planetary boundary layer (PBL). Data have not been corrected for this effect. Sonde releases were generally at the same time of day at each site, but there was some variation in release time between sites (generally mid-afternoon, but in some cases at synoptic times). Sounding frequency varied from daily (at four sites) to as little as weekly (one site).

Table 1. INTEX Ozonesonde Network Study sites for July 1–Aug.15, 2004 study period.

Sounding Site	Location	Altitude, m	# of Profiles	Release Time
Ron Brown research vessel	Gulf of Maine (~ 43.27 N, 69.70 W)	0	33	15z
Beltsville, MD, USA	39.04 N, 76.52 W	24	8	14z
Boulder, CO, USA	40.30 N, 105.20 W	1743	7	17z
Egbert, ON, CAN	44.23 N, 79.78 W	251	5	11z
Houston, TX, USA	29.72 N, 95.40 W	19	25	19z
Huntsville, AL, USA	35.28 N, 86.58 W	196	14	19z
Narragansett, RI, USA	41.49 N, 71.42 W	21	39	18z
Pellston, MI, USA	45.57 N, 84.68 W	235	38	18z
Sable I., NS., CAN	43.93 N, 60.01 W	4	33	23z
Trinidad Head, CA, USA	40.80 N, 124.15 W	20	40	18z
Wallops I., VA, USA	37.85 N, 75.50 W	13	18	17z
Yarmouth, NS., CAN	43.87 N, 66.12 W	9	15	17z

2.2 Model descriptions

CHRONOS is a chemical transport model (CTM) that was developed originally by EC to provide guidance to Canadian policymakers on managing photochemical oxidants. More recently it has been used operationally by EC to issue short-term (48-hour) public forecasts of ozone (since 2001) and $PM_{2.5}$ (since 2004) concentrations. The CHRONOS operational domain covers most of the North American continent (see Figure 1). In the horizontal a 350x250 grid with 21-km grid-cell spacing is used on a polar-stereographic map projection; in the vertical 24 Gal-Chen terrain-following levels are used with a top at 6 km. The advection scheme used for tracer transport is a non-oscillatory, semi-Lagrangian scheme [*Pudykiewicz et al.,* 1997; *Sirois et al.,* 1999]. Vertical diffusion is treated via a turbulence kinetic energy closure scheme using a

first-order solver. The ADOM-II gas-phase chemistry mechanism used by CHRONOS considers 114 chemical reactions and 47 species [*Pudykiewicz et al.,* 1997]. Dry deposition of gases is based on a resistance parameterization with the dry deposition velocity of each dry-depositing species parameterized as a weighted combination of two master species, SO_2 and O_3: 13 gaseous species are assumed to dry deposit [*Zhang et al,* 2002]. A simple two-section particle size distribution (diameter ranges of 0-2.5 μm and 2.5-10 μm) is employed to represent particulate matter (PM). Secondary organic aerosol formation is parameterized based on a scheme proposed by *Pandis et al*. [1992]. Treatment of size-dependant particle dry deposition and sedimentation is based on *Zhang et al.* [2001]. For inorganic heterogeneous chemistry (gas-particle partitioning of H_2SO_4, HNO_3, and NH_3), a numerically efficient and stable code based on the ISORROPIA algorithms that was developed for AURAMS is used [*Makar et al.,* 2003a]. However, aqueous-phase chemistry is not considered.

CHRONOS was also used as the starting point for AURAMS, a more comprehensive AQ model designed to treat photochemical oxidants and acid deposition, and particulate matter (PM). As a consequence, CHRONOS and AURAMS share the same grid structure, advection scheme, gas-phase chemical mechanism, inorganic heterogeneous chemistry scheme, meteorological driver, and anthropogenic emissions inputs, but AURAMS also contains considerably more detailed treatments of aerosol kinetics and chemistry as well as some other process representations not included in CHRONOS. AURAMS employs a sectional approach to represent the size distribution and chemical composition of atmospheric PM. Twelve size bins span the diameter size range from 0.01 to 40.96 μm and the following aerosol processes are considered: emissions; nucleation; condensation; coagulation; hygroscopic growth; dry deposition/sedimentation; aerosol activation; and below-cloud scavenging [*Gong et al.,* 2003a]. Up to nine PM chemical

components are considered: sulphate; nitrate; ammonium; black carbon; primary organic matter; secondary organic matter; crustal material; sea salt; and particle-bound water. The AURAMS aqueous-phase chemistry mechanism includes 20 reactions, including mass transfer and aqueous-phase sulphur oxidation: 13 aqueous-phase species are considered, and nucleation scavenging of aerosols by cloud droplets is directly linked to aerosol activation [*Gong et al,* 2006]. Sea-salt emission from wave-breaking is modelled on-line [*Gong et al.,* 2003a]. Secondary organic aerosol formation is parameterized using one of two schemes [*Odum et al.,* 1996; *Jiang et al.*, 2003]. A second-order scheme is used to treat vertical diffusion. Plume rise is considered for major point sources. Wet deposition includes the removal of soluble gases and aerosols by cloud-to-rain conversion and below-cloud scavenging (impact scavenging of aerosols, reversible and irreversible scavenging of gases), and below-cloud evaporation is also considered [*Gong et al.,* 2006]. Mass-consistency and mass-conservation corrections are also applied [*Gong et al*., 2003b].

2.3 Model runs during ICARTT

CHRONOS forecasts were readily available during ICARTT since the model was run operationally throughout 2004 at the Canadian Meteorological Centre in Montreal, Quebec. In order to participate in ICARTT, a special real-time AURAMS run was set up to complement the operational CHRONOS run. The AURAMS domain used for ICARTT covered eastern North America (Figure 1). In the horizontal, a 85x105 grid with 42-km grid-cell spacing was used on the same polar-stereographic map projection as CHRONOS; in the vertical, 28 vertical levels with a top at 29 km were used. Each AURAMS 48-hr forecast was launched at 00 UTC daily

using the previous day's forecast at 24 hours to specify the initial atmospheric chemical state. The AURAMS integration time step was 450 s while the CHRONOS time step was 3600 s.

Both CHRONOS and AURAMS are off-line CTMs that are driven by the Canadian operational weather forecast model, GEM (Global Environmental Multiscale model). GEM is a non-hydrostatic, two-time-level, semi-implicit, semi-Lagrangian model [*Côté et al.,* 1998a,b]. For AQ applications, meteorological fields from a high-resolution regional window positioned over the AQ modelling domain are stored at the frequency required by the CTM. For the ICARTT runs both models used meteorological fields from GEM version 3.1.2, but with 15-km horizontal grid spacing for CHRONOS vs. 24 km for AURAMS.

Both models used emission fields that were based on the 1990 Canadian and U.S. national criteria air contaminant inventories scaled to 1995 and 1996 levels by Canadian province and U.S. state, respectively. The Canadian Emissions Processing System was used to prepare hourly point-, area-, mobile-, and biogenic-source emission fields on the CHRONOS grid shown in Figure 1 from these inventories, including 17 gas-phase species and primary bulk PM2.5 and PM10 emissions [e.g., *Scholtz et al.,* 1999; *Makar et al.,* 2003b]. AURAMS used the same emissions fields but aggregated to its 42-km grid. Biogenic emissions of NOx and VOCs were calculated "on-line" in CHRONOS using BEIS2 algorithms and BELD3 vegetation database [*Pierce et al*., 1998; *Kinnee et al*., 2005] and meteorological fields from GEM, whereas in AURAMS biogenic emissions were calculated off-line using BEIS2 algorithms but an older, less detailed BEIS1 vegetation database. The advantage of the BEIS1 vegetation database was its use of the same vegetation classes in both Canada and the U.S., unlike the BELD3 data set, which contains much more detail for the U.S.

2.4 Additional model runs

The CHRONOS and AURAMS runs made during the ICARTT field experiment in 2004 will be referred to hereafter as the CHRONOS-OP (short for "operational") and AURAMS-RT (short for "real-time") runs. Three additional runs for the ICARTT period made using modified versions of CHRONOS and AURAMS are also considered here. During ICARTT, in addition to the operational CHRONOS 48-hr forecast, an experimental 48-hr forecast with assimilation of near-real time surface O_3 data was generated at 00 UTC. This version of CHRONOS had 24 levels with a top at 8 km. Assimilation of surface O_3 data was for a 3 hour period, from 12 UTC to 15 UTC. This second CHRONOS version will be referred to CHRONOS-SDA (surface data assimilation).

One significant difference between CHRONOS-OP and AURAMS-RT was in the treatment of biogenic emissions. Following the ICARTT experiment, a comparison of CHRONOS and AURAMS predictions of free-tropospheric isoprene concentrations vs. aircraft measurements showed the AURAMS values to be significantly lower than both the CHRONOS values and the aircraft measurements (*McKeen*, 2005). Since biogenic sources are the dominant source of atmospheric isoprene, an ozone precursor, a second run of AURAMS was carried out after implementation of an improved treatment of biogenic emissions based on the BEIS3 (version 3.09) algorithms [*U.S. EPA*, 2001] and the BELD3 vegetation database. This second AURAMS run will be referred to as the AURAMS-BIO (biogenic) run.

The third additional run will be referred to as the AURAMS-NEW run and was performed with a newer version of AURAMS. The AURAMS-RT and AURAMS-BIO ICARTT simulations were both run using AURAMS version 1.1, whereas the AURAMS-NEW run was made using version

1.3.1. New features in version 1.3.1 include the treatment of CO as a prognostic species rather than as fixed, horizontally-homogeneous field, the implementation of a more accurate solver for vertical diffusion, the use of the *Jiang* [2003] scheme for secondary organic aerosol formation instead of the *Odum et al*. [1996] scheme, and the same treatment of biogenic emissions as in the AURAMS-BIO run. The pseudo-1995/96 anthropogenic emission files used by the other four CHRONOS and AURAMS runs were replaced by an updated set of emissions files generated from the 2000 Canadian and 2001 U.S. national emission inventories using the SMOKE emissions processing system (version 2.1) [see *Carolina Environmental Program*, 2006]. In addition, a newer version of the GEM weather forecast model (version 3.2.1 plus a treatment of urban heat fluxes following *Makar et al.* [2006]) was used to prepare input meteorological fields.

Considering the set of five model versions that were used, the CHRONOS-OP and CHRONOS-SDA pair differed in two main respects – the use of surface data assimilation and the extension of the domain in the vertical from 6 to 8 km – and the AURAMS-RT and AURAMS-BIO pair differed in only one respect – the change in the treatment of biogenic emissions. Comparing CHRONOS and AURAMS, the CHRONOS-OP and AURAMS-BIO versions were the most similar, and AURAMS-NEW was the most different from all of the other versions.

3. Profile Comparisons

Several different comparisons of the 275 IONS ozone soundings with CHRONOS and AURAMS predictions are presented in this section. Six examples of model forecasts compared with single ozone soundings are shown in Figures 2 to 7. These examples have been chosen to illustrate different features of model performance, and are not necessarily representative of average performance. Average observed and predicted ozone profiles are compared at each

IONS sounding site, and some statistics are presented in Tables 2-6. Time series comparisons at 0 and 1000m are shown in Figures 8 and 9, and differences in the upper troposphere are examined in Figure 10.

3.1 Lower troposphere

Figure 2 compares an early-morning ozone sounding (11 UTC/6 LST) on July 14th, 2004 at Egbert, Ontario with the predicted ozone profiles from the five model versions for that time and location (obtained by bilinear interpolation in the horizontal). The sharp transition ozone concentration in the vertical from the surface through the nocturnal inversion to the residual layer above is captured by the models, although in all cases the vertical gradient is apparently overestimated. This may be due in part to the response time of the ozone sensor (see Section 2.l), since this will tend to smooth the observed profile. The true ozone profile below 1 km may therefore more closely resemble that forecast by the models than it would appear from this comparison. The two CHRONOS runs also reproduce the secondary feature at 2000 m.

Figure 3 shows an evening sounding (23 UTC/19 LST) on July 30th at Sable Island, Nova Scotia. The boundary layer transition in the vertical is less pronounced for this case. The three AURAMS runs predict this low-level feature well, though two are biased low overall and one high overall. The two CHRONOS runs, on the other hand, predict much more pronounced PBL effects than are seen in the measurements. On the other hand, all of the models are low, relative to the sonde, above 3000 m. Similar behaviour above 3000 m is apparent in Figures 4-7, and as discussed in Section 3.2 this bias becomes more pronounced at higher altitudes.

An early-afternoon sounding (17 UTC/13 LST) on July 30th at Yarmouth, Nova Scotia (Figure 4), shows a shallow layer of high ozone molar mixing ratio at 500 m, just above the top of the

marine boundary layer. The two CHRONOS runs predict this feature fairly well, with the operational version (CHRONOS-OP) doing a somewhat better job of reproducing the narrowness of the layer, while the version with assimilation of surface ozone data (CHRONOS-SDA) correctly places the altitude of the layer. The three AURAMS runs are all quite different among themselves but all predict a broader feature and all are biased low.

In Figure 5 the early-afternoon ozone profile (20 UTC/14 LST) for July 16th at Huntsville, Alabama shows a deep (2 km) boundary layer of photochemically-produced ozone. All five model versions predict large ozone production in this layer, and all get the PBL depth about right, but none predicts the ozone increase from the surface to 1500 m. As a result the AURAMS run results are much closer to the sonde measurement at the surface, whereas the CHRONOS run results are close to the sonde value at the top of the PBL (1500 m). All of the models underpredict ozone values above 3000 m, the AURAMS runs especially so.

Similarly, for the early-afternoon ozone profile (18 UTC/13 LST) on August 10th at Narragansett, Rhode Island (Figure 6), all of the models predict high ozone levels near the surface, although they underpredict higher up. The assimilation of surface ozone data appears to have distorted the CHRONOS profile in this case, as the CHRONOS-OP run is a much better fit to the measured data than is the CHRONOS-SDA run. All of the model runs except CHRONOS-SDA show some similarity to the observed "two-step" structure in the first 1500 m.

In Figure 7, the early-afternoon sounding (19 UTC/14 LST) for July 7th at Wallops Island, Virginia shows a very complex, multi-layered ozone profile. Four of the model versions predict the ozone maximum at 700 m. One run (CHRONOS-SDA) also shows some indication of the

secondary peak at 2000 m. The AURAMS-NEW profile is quite different from the others and does not predict any layering above 500 m.

A statistical summary of overall model performance in predicting the IONS ozone profiles is given in Tables 2-6 for model versions AURAMS-RT, AURAMS-BIO, AURAMS-NEW, CHRONOS-OP and CHRONOS-SDA, respectively. Calculated biases are variable, and in some cases quite modest. Differences in sonde preparation between stations (Section 2.1) may contribute a minor part of the station-to-station variation in model-sonde bias. Model-sonde differences for individual profiles, however, are often large, as evidenced by the quoted uncertainties (one standard deviation), which are generally in the range of 10-30 ppbv, or 25-75% of typical tropospheric ozone amounts. Over all sites, in the first 1000 m, both biases and standard deviations are lowest for the AURAMS-RT run. The surface ozone data assimilation appears to reduce both biases and standard deviations for CHRONOS (Tables 5 and 6), although for some sites actual surface biases increase (e.g., Huntsville, where the bias in Table 6 is the largest surface-level bias of any of the models, at any site). In general, agreement in the first 1000 m is best at Egbert, Yarmouth, Pellston and Sable Island, that is, at the northernmost IONS stations (see Figure 1). One possible explanation is that the Canadian emissions used as input to CHRONOS and AURAMS were more accurate than those for the U.S. Interestingly, implementation of pollutant control legislation in the U.S. ("NO_x SIP Call") resulted in a significant reduction in U.S. NO_x emissions occurring between 2001 and 2004, after the applicable years for the two U.S. emission inventories that were used for these runs [*Frost et al.,* 2006]. The biases in Tables 2-6 at US sites in the lowest 1000m are predominantly overpredictions, and this may be partly due to the reduction in actual vs forecast emissions. In addition, several of the US sites (Beltsville, Houston, Narragansett) are near or downwind of

Table 2. Model-sonde average differences in ppb for AURAMS-RT run. Quoted uncertainties correspond to one standard deviation. The number after each ozone site name indicates the number of profiles considered. No values are given for Boulder and Trinidad Head because these sites are located outside of the AURAMS domain.

Height (m)	Beltsville (8)	Boulder (7)	Egbert (5)	Houston (25)	Huntsville (14)	Narragansett (39)
5	-14.2 ± 22		-5.8 ± 10	-2.5 ± 18	0.9 ± 10	8.9 ± 19
20	-15.9 ± 22		-2.1 ± 8.	-7.5 ± 19	-3.9 ± 13	9.9 ± 19
60	-14.9 ± 21		0.5 ± 9.	-7.0 ± 19	-3.6 ± 14	9.8 ± 20
125	-14.6 ± 19		-3.7 ± 7.	-7.4 ± 20	-4.5 ± 13	8.7 ± 20
200	-13.5 ± 17		-7.4 ± 8.	-7.8 ± 20	-5.9 ± 14	7.5 ± 20
290	-11.1 ± 17		-6.1 ± 9.	-8.4 ± 20	-7.1 ± 15	5.8 ± 21
395	-9.3 ± 17		-3.2 ± 13	-9.0 ± 20	-7.6 ± 15	3.4 ± 20
515	-8.7 ± 17		-0.8 ± 14	-9.4 ± 20	-8.1 ± 16	0.9 ± 19
655	-8.4 ± 17		0.0 ± 15	-10.3 ± 20	-8.8 ± 15	-2.6 ± 21
820	-10.8 ± 17		0.8 ± 13	-10.4 ± 21	-9.8 ± 15	-4.9 ± 22
1015	-14.1 ± 18		-0.7 ± 13	-10.8 ± 23	-10.6 ± 15	-6.2 ± 23
1240	-19.7 ± 16		-2.1 ± 18	-11.6 ± 23	-11.1 ± 14	-9.3 ± 22
1505	-21.9 ± 14		-2.9 ± 22	-20.8 ± 19	-13.8 ± 11	-13.8 ± 20
1815	-23.7 ± 11		-5.3 ± 23	-29.5 ± 19	-24.4 ± 14	-21.0 ± 18
2175	-28.6 ± 10		-9.5 ± 22	-40.4 ± 27	-36.1 ± 20	-27.8 ± 17
2595	-35.9 ± 14		-17.8 ± 25	-47.7 ± 20	-49.0 ± 19	-35.2 ± 16
3090	-43.9 ± 15		-24.3 ± 21	-53.9 ± 19	-50.5 ± 15	-43.5 ± 14

Height (m)	Pellston (38)	RHBrown (34)	Sable (33)	Trinidad (40)	Wallops (18)	Yarmouth (15)
5	-8.8 ± 15	10.8 ± 16	-11.8 ± 10		3.5 ± 15	-8.2 ± 9.
20	-9.9 ± 15	10.7 ± 17	-12.2 ± 11		3.2 ± 15	-8.2 ± 9.
60	-10.2 ± 15	14.6 ± 19	-13.0 ± 11		2.7 ± 15	-9.1 ± 9.
125	-10.9 ± 15	13.6 ± 21	-13.8 ± 11		1.2 ± 15	-10.1 ± 9.
200	-11.5 ± 16	11.9 ± 20	-14.1 ± 11		0.5 ± 15	-11.9 ± 9.
290	-12.0 ± 15	10.3 ± 19	-14.3 ± 12		-0.6 ± 15	-11.6 ± 9.
395	-12.6 ± 15	7.4 ± 18	-13.9 ± 13		-0.9 ± 15	-12.8 ± 11
515	-13.2 ± 16	4.8 ± 18	-14.1 ± 12		-2.0 ± 15	-12.6 ± 11
655	-13.9 ± 16	4.1 ± 19	-15.2 ± 13		-3.9 ± 15	-11.5 ± 14
820	-15.2 ± 16	2.4 ± 18	-17.1 ± 14		-5.3 ± 14	-11.8 ± 14
1015	-17.7 ± 16	-2.7 ± 18	-19.4 ± 14		-9.0 ± 12	-14.9 ± 12
1240	-22.1 ± 15	-9.7 ± 19	-21.7 ± 14		-11.7 ± 12	-18.1 ± 12
1505	-27.4 ± 16	-15.0 ± 18	-25.1 ± 13		-15.8 ± 11	-20.5 ± 11
1815	-33.2 ± 15	-20.4 ± 17	-27.3 ± 12		-20.7 ± 13	-24.5 ± 11
2175	-40.6 ± 16	-24.8 ± 15	-29.7 ± 13		-24.4 ± 13	-31.6 ± 11
2595	-46.1 ± 14	-30.6 ± 14	-33.4 ± 14		-33.2 ± 15	-37.2 ± 14
3090	-51.1 ± 13	-35.7 ± 14	-36.6 ± 14		-40.5 ± 16	-42.7 ± 13

Table 3. Model-sonde average differences in ppb for AURAMS-BIO ICARTT run. Quoted uncertainties correspond to one standard deviation.

Height (m)	Beltsville (8)	Boulder (7)	Egbert (5)	Houston (25)	Huntsville (14)	Narragansett (39)
5	11.7 ± 35		-2.1 ± 11	16.0 ± 24	3.0 ± 6.	18.8 ± 22
20	10.1 ± 34		2.0 ± 9.	11.1 ± 25	-2.8 ± 9.	19.7 ± 23
60	11.4 ± 32		5.2 ± 10	11.9 ± 24	-2.7 ± 10	19.6 ± 23
125	12.1 ± 29		1.0 ± 9.	11.8 ± 24	-3.7 ± 10	18.2 ± 23
200	13.2 ± 26		-2.6 ± 9.	11.4 ± 25	-5.3 ± 11	17.1 ± 23
290	14.2 ± 24		-0.9 ± 11	10.9 ± 25	-6.7 ± 12	15.6 ± 22
395	14.2 ± 23		2.5 ± 16	10.4 ± 25	-7.3 ± 12	13.1 ± 21
515	12.6 ± 21		5.2 ± 16	9.9 ± 24	-7.7 ± 13	10.3 ± 20
655	11.0 ± 21		6.5 ± 17	9.0 ± 22	-8.3 ± 13	5.8 ± 22
820	6.3 ± 20		7.4 ± 14	9.2 ± 22	-9.2 ± 12	2.5 ± 24
1015	1.1 ± 21		5.8 ± 12	8.2 ± 23	-9.9 ± 12	0.8 ± 25
1240	-7.0 ± 19		4.3 ± 16	6.1 ± 25	-9.8 ± 11	-3.0 ± 23
1505	-10.2 ± 17		4.2 ± 23	-5.4 ± 21	-17.9 ± 14	-8.4 ± 21
1815	-12.8 ± 12		1.8 ± 25	-19.2 ± 17	-21.6 ± 17	-15.5 ± 19
2175	-19.8 ± 11		-3.9 ± 25	-35.7 ± 27	-38.0 ± 22	-22.7 ± 18
2595	-30.7 ± 16		-13.5 ± 28	-44.5 ± 21	-51.2 ± 15	-31.3 ± 17
3090	-40.0 ± 17		-20.0 ± 25	-51.8 ± 19	-53.0 ± 13	-40.3 ± 15

Height (m)	Pellston (38)	RHBrown (34)	Sable (33)	Trinidad (40)	Wallops (18)	Yarmouth (15)
5	-7.4 ± 17	16.9 ± 19	-10.2 ± 11		12.7 ± 18	-4.1 ± 13
20	-8.6 ± 17	17.0 ± 20	-10.5 ± 11		12.6 ± 18	-2.3 ± 13
60	-9.0 ± 17	21.5 ± 23	-11.3 ± 12		12.3 ± 19	0.2 ± 14
125	-9.8 ± 17	20.8 ± 24	-12.1 ± 12		10.5 ± 18	1.3 ± 14
200	-10.4 ± 17	18.7 ± 24	-12.3 ± 12		9.8 ± 18	0.5 ± 14
290	-11.1 ± 17	16.8 ± 23	-12.3 ± 14		8.6 ± 18	-2.8 ± 15
395	-11.7 ± 17	14.1 ± 22	-11.7 ± 15		8.4 ± 18	-5.2 ± 18
515	-12.4 ± 17	11.9 ± 22	-11.8 ± 14		7.5 ± 18	-6.4 ± 16
655	-13.1 ± 17	11.4 ± 22	-12.8 ± 14		5.7 ± 17	-6.2 ± 17
820	-14.1 ± 17	9.7 ± 21	-14.8 ± 15		5.1 ± 17	-7.1 ± 18
1015	-17.0 ± 16	4.0 ± 20	-16.9 ± 16		1.6 ± 15	-10.3 ± 19
1240	-21.5 ± 16	-3.8 ± 21	-19.1 ± 16		-1.5 ± 16	-13.0 ± 18
1505	-26.8 ± 17	-9.6 ± 21	-22.3 ± 15		-6.6 ± 15	-15.6 ± 16
1815	-32.3 ± 15	-15.2 ± 19	-24.3 ± 14		-13.5 ± 17	-20.7 ± 17
2175	-39.7 ± 16	-19.7 ± 17	-26.5 ± 15		-19.0 ± 16	-25.8 ± 18
2595	-46.2 ± 13	-25.8 ± 16	-30.0 ± 16		-29.3 ± 17	-28.2 ± 18
3090	-51.8 ± 12	-31.4 ± 16	-33.0 ± 16		-37.3 ± 19	-32.3 ± 16

Table 4. Model-sonde average differences in ppb for AURAMS-NEW ICARTT run. Quoted uncertainties correspond to one standard deviation.

Height (m)	Beltsville (8)	Boulder (7)	Egbert (5)	Houston (25)	Huntsville (14)	Narragansett (39)
5	3.1 ± 20		0.4 ± 14	-8.8 ± 17	2.9 ± 9.	15.4 ± 19
20	1.7 ± 21		2.9 ± 11	-11.3 ± 18	-2.0 ± 10	17.6 ± 20
60	2.2 ± 20		2.1 ± 9.	-9.5 ± 18	-1.2 ± 11	17.4 ± 20
125	1.2 ± 20		-3.4 ± 7.	-9.1 ± 18	-2.1 ± 11	16.4 ± 20
200	0.2 ± 18		-3.6 ± 9.	-8.8 ± 19	-3.9 ± 12	15.5 ± 20
290	-0.1 ± 18		-0.2 ± 11	-8.5 ± 19	-5.2 ± 12	13.6 ± 20
395	1.0 ± 16		0.8 ± 13	-8.6 ± 20	-5.8 ± 13	10.1 ± 20
515	1.9 ± 14		1.9 ± 13	-8.5 ± 19	-6.4 ± 13	6.9 ± 21
655	1.5 ± 13		1.6 ± 13	-9.2 ± 18	-7.1 ± 13	3.2 ± 22
820	0.0 ± 12		2.4 ± 9.	-9.2 ± 18	-8.1 ± 13	1.5 ± 22
1015	-2.0 ± 11		1.4 ± 7.	-8.6 ± 19	-8.9 ± 12	1.4 ± 22
1240	-6.0 ± 14		-1.9 ± 7.	-7.0 ± 19	-9.1 ± 11	1.2 ± 21
1505	-8.3 ± 15		-5.1 ± 9.	-4.7 ± 20	-11.1 ± 8.	0.2 ± 19
1815	-8.9 ± 15		-8.2 ± 13	-3.1 ± 21	-15.3 ± 15	-3.6 ± 18
2175	-10.0 ± 11		-10.2 ± 14	-1.7 ± 20	-17.3 ± 17	-9.2 ± 16
2595	-9.7 ± 11		-14.7 ± 21	-2.4 ± 16	-25.1 ± 15	-16.1 ± 14
3090	-16.4 ± 9.		-18.1 ± 18	-22.3 ± 15	-31.0 ± 9.	-23.3 ± 14

Height (m)	Pellston (38)	RHBrown (34)	Sable (33)	Trinidad (40)	Wallops (18)	Yarmouth (15)
5	-0.8 ± 16	21.8 ± 18	-3.1 ± 14		11.3 ± 19	3.6 ± 13
20	-1.2 ± 15	21.6 ± 19	-3.5 ± 14		11.4 ± 19	7.6 ± 15
60	-1.4 ± 15	24.6 ± 22	-4.1 ± 15		11.5 ± 19	9.1 ± 16
125	-2.1 ± 15	22.7 ± 22	-4.7 ± 15		9.9 ± 18	9.2 ± 17
200	-2.7 ± 15	20.3 ± 22	-4.7 ± 16		9.0 ± 19	7.6 ± 17
290	-3.2 ± 15	18.2 ± 21	-4.9 ± 17		8.4 ± 19	3.9 ± 18
395	-3.7 ± 15	15.3 ± 20	-4.2 ± 17		8.3 ± 18	0.4 ± 20
515	-4.1 ± 15	12.5 ± 19	-4.3 ± 17		7.0 ± 18	-1.3 ± 19
655	-4.4 ± 15	10.8 ± 18	-5.4 ± 17		4.7 ± 19	-1.2 ± 19
820	-5.4 ± 15	9.2 ± 17	-7.0 ± 18		3.2 ± 18	-1.5 ± 20
1015	-7.4 ± 14	6.3 ± 17	-8.8 ± 19		1.6 ± 17	-3.6 ± 21
1240	-9.7 ± 12	2.5 ± 18	-10.8 ± 19		-0.6 ± 17	-6.2 ± 20
1505	-12.7 ± 11	-0.1 ± 18	-14.1 ± 18		-2.3 ± 18	-9.2 ± 19
1815	-16.0 ± 11	-3.5 ± 17	-16.2 ± 16		-5.5 ± 19	-13.7 ± 19
2175	-21.0 ± 14	-7.5 ± 15	-18.4 ± 15		-6.9 ± 18	-18.4 ± 17
2595	-25.3 ± 14	-11.8 ± 15	-21.1 ± 16		-12.8 ± 17	-20.9 ± 16
3090	-29.5 ± 13	-16.3 ± 14	-23.0 ± 16		-19.2 ± 16	-24.4 ± 15

Table 5. Model-sonde average differences in ppb for CHRONOS-OP, during ICARTT. Quoted uncertainties correspond to one standard deviation.

Height (m)	Beltsville (8)	Boulder (7)	Egbert (5)	Houston (25)	Huntsville (14)	Narragansett (39)
0	14.3 ± 31	12.9 ± 21	-6.8 ± 20	2.9 ± 23	19.2 ± 19	17.4 ± 17
10	11.8 ± 32	10.5 ± 21	-4.9 ± 19	-2.7 ± 24	15.5 ± 11	17.7 ± 17
50	12.5 ± 31	9.6 ± 21	3.4 ± 20	-2.2 ± 24	18.1 ± 9.	17.7 ± 17
100	11.9 ± 30	8.5 ± 22	1.7 ± 19	-2.4 ± 25	15.6 ± 8.	16.6 ± 17
200	11.1 ± 29	7.8 ± 22	3.2 ± 9.	-2.6 ± 25	13.0 ± 9.	15.5 ± 18
300	12.5 ± 27	6.5 ± 21	4.6 ± 10	-3.2 ± 25	10.9 ± 9.	13.7 ± 20
400	13.2 ± 25	4.2 ± 19	5.1 ± 10	-3.8 ± 25	9.6 ± 10	11.6 ± 21
500	10.2 ± 27	3.6 ± 18	1.8 ± 10	-4.0 ± 24	8.5 ± 10	9.7 ± 21
600	6.7 ± 30	3.5 ± 16	2.9 ± 12	-4.9 ± 24	7.8 ± 10	7.8 ± 21
700	3.9 ± 32	3.7 ± 14	2.1 ± 13	-5.5 ± 25	7.1 ± 11	6.1 ± 21
800	2.3 ± 32	-1.8 ± 12	-0.3 ± 12	-5.7 ± 26	6.4 ± 11	5.6 ± 22
900	3.1 ± 30	-1.9 ± 12	0.4 ± 13	-5.9 ± 26	5.8 ± 11	6.0 ± 22
1000	2.1 ± 29	-0.9 ± 10	0.5 ± 14	-7.6 ± 23	4.5 ± 11	5.0 ± 21
1200	-6.2 ± 22	-4.5 ± 10	1.5 ± 16	-9.6 ± 23	3.7 ± 10	2.6 ± 19
1500	-12.3 ± 19	-7.3 ± 12	1.7 ± 15	-16.3 ± 24	0.1 ± 10	-1.7 ± 17
2000	-15.7 ± 18	-9.0 ± 15	0.8 ± 14	-18.2 ± 26	-5.0 ± 8.	-5.4 ± 17
2500	-20.2 ± 10	-8.9 ± 14	-4.8 ± 13	-13.4 ± 17	-12.0 ± 9.	-11.5 ± 13
3000	-23.9 ± 8.	-8.7 ± 13	-4.0 ± 16	-14.7 ± 18	-11.1 ± 8.	-14.5 ± 13

Height (m)	Pellston (38)	RHBrown (34)	Sable (33)	Trinidad (40)	Wallops (18)	Yarmouth (15)
0	5.0 ± 11	13.8 ± 20	-0.1 ± 9	11.5 ± 12	15.3 ± 15	5.5 ± 14
10	3.9 ± 11	11.7 ± 20	-0.3 ± 9	10.1 ± 13	15.2 ± 15	5.9 ± 14
50	3.8 ± 11	17.3 ± 21	0.8 ± 9	9.6 ± 12	14.7 ± 15	6.8 ± 15
100	3.1 ± 10	17.1 ± 21	1.6 ± 10	8.6 ± 12	13.4 ± 15	6.9 ± 14
200	2.1 ± 10	13.9 ± 21	3.0 ± 12	7.4 ± 12	12.4 ± 15	6.2 ± 14
300	1.3 ± 10	9.5 ± 17	4.3 ± 15	8.4 ± 14	11.7 ± 14	1.7 ± 13
400	1.1 ± 10	7.4 ± 15	3.8 ± 15	9.0 ± 15	12.0 ± 14	-1.9 ± 12
500	0.8 ± 11	5.7 ± 15	4.5 ± 14	8.6 ± 14	10.9 ± 14	-3.7 ± 12
600	0.4 ± 11	4.5 ± 15	4.4 ± 13	8.1 ± 13	8.7 ± 14	-3.1 ± 12
700	0.2 ± 11	3.8 ± 16	4.4 ± 13	7.7 ± 13	7.9 ± 14	-2.4 ± 14
800	0.5 ± 11	2.8 ± 16	3.4 ± 14	6.5 ± 14	5.3 ± 12	-2.0 ± 16
900	0.6 ± 11	1.7 ± 17	3.1 ± 15	4.7 ± 14	3.3 ± 12	-3.2 ± 17
1000	-0.2 ± 11	0.4 ± 18	2.7 ± 16	2.9 ± 14	1.5 ± 12	-5.3 ± 17
1200	-1.9 ± 11	-2.9 ± 19	2.9 ± 17	0.8 ± 14	0.1 ± 13	-7.8 ± 16
1500	-5.0 ± 10	-6.9 ± 16	-0.3 ± 15	-3.1 ± 14	-2.7 ± 12	-9.5 ± 18
2000	-9.2 ± 9.	-9.9 ± 15	-0.5 ± 14	-2.9 ± 14	-6.6 ± 13	-12.4 ± 14
2500	-13.0 ± 10	-14.2 ± 12	-2.1 ± 15	-4.3 ± 13	-11.3 ± 13	-14.4 ± 11
3000	-15.5 ± 10	-17.2 ± 12	-6.2 ± 14	-7.5 ± 15	-16.0 ± 11	-13.5 ± 11

Table 6. Model-sonde average differences in ppb for for CHRONOS-SDA, with assimilation of surface ozone observations. Quoted uncertainties correspond to one standard deviation.

Height (m)	Beltsville (8)	Boulder (7)	Egbert (5)	Houston (25)	Huntsville (14)	Narragansett (39)
0	6.2 ± 31	11.4 ± 15	-5.4 ± 17	2.4 ± 20	23.7 ± 12	10.6 ± 15
10	3.7 ± 32	9.1 ± 16	-2.1 ± 16	-2.9 ± 22	17.3 ± 12	10.8 ± 15
50	3.5 ± 31	8.2 ± 16	4.5 ± 22	-2.3 ± 21	16.9 ± 12	10.8 ± 15
100	2.6 ± 30	7.1 ± 16	2.0 ± 24	-2.8 ± 22	15.5 ± 12	9.7 ± 16
200	1.3 ± 29	6.4 ± 16	-2.8 ± 19	-3.2 ± 22	14.1 ± 12	8.2 ± 17
300	3.8 ± 26	5.3 ± 15	0.4 ± 12	-3.9 ± 21	12.3 ± 12	6.3 ± 18
400	6.5 ± 24	3.2 ± 13	8.8 ± 14	-4.4 ± 21	11.4 ± 13	4.5 ± 18
500	5.6 ± 25	1.8 ± 12	13.5 ± 18	-4.7 ± 21	10.6 ± 13	3.7 ± 18
600	5.7 ± 25	0.8 ± 12	10.5 ± 19	-5.7 ± 21	10.0 ± 13	3.3 ± 18
700	4.4 ± 27	0.8 ± 11	8.4 ± 20	-6.8 ± 20	9.1 ± 13	3.6 ± 18
800	4.3 ± 25	0.5 ± 10	8.0 ± 21	-6.9 ± 20	8.1 ± 12	3.7 ± 18
900	3.6 ± 24	0.9 ± 9.	6.9 ± 22	-7.1 ± 21	6.4 ± 12	4.4 ± 19
1000	-0.7 ± 24	0.1 ± 9.	5.1 ± 22	-6.5 ± 21	5.1 ± 11	3.5 ± 20
1200	-7.6 ± 26	-4.2 ± 10	4.6 ± 22	-8.0 ± 21	3.8 ± 10	0.8 ± 20
1500	-13.4 ± 24	-4.7 ± 8.	3.2 ± 21	-15.6 ± 21	-0.1 ± 7.	-3.6 ± 18
2000	-22.6 ± 15	-7.8 ± 9.	2.9 ± 21	-19.0 ± 20	-3.4 ± 13	-8.5 ± 15
2500	-18.6 ± 9.	-9.1 ± 9.	-7.0 ± 17	-14.7 ± 14	-12.3 ± 8.	-13.9 ± 13
3000	-23.7 ± 10	-10.3 ± 8.	-11.3 ± 15	-13.7 ± 14	-11.8 ± 10	-16.4 ± 10

Height (m)	Pellston (38)	RHBrown (34)	Sable (33)	Trinidad (40)	Wallops (18)	Yarmouth (15)
0	2.4 ± 8.	4.9 ± 16	-10.2 ± 8.	14.2 ± 12	8.9 ± 14	0.2 ± 11
10	1.3 ± 8.	3.2 ± 16	-10.4 ± 8.	13.2 ± 12	8.8 ± 14	0.4 ± 10
50	1.3 ± 8.	7.9 ± 16	-10.3 ± 9.	13.0 ± 12	8.9 ± 13	-0.4 ± 10
100	0.6 ± 8.	6.8 ± 16	-10.5 ± 9.	12.0 ± 12	7.7 ± 13	-1.1 ± 10
200	-0.2 ± 8.	5.5 ± 16	-9.3 ± 9.	10.9 ± 12	6.7 ± 12	-2.6 ± 10
300	-0.6 ± 8.	3.5 ± 15	-4.6 ± 11	10.9 ± 14	5.5 ± 12	-5.1 ± 8.
400	-1.0 ± 9.	1.8 ± 14	-0.2 ± 13	11.9 ± 16	5.0 ± 11	-3.4 ± 12
500	-1.1 ± 9.	0.9 ± 14	1.5 ± 14	11.1 ± 16	4.6 ± 11	-4.5 ± 14
600	-1.3 ± 10	0.4 ± 13	2.5 ± 15	9.6 ± 15	4.1 ± 11	-3.8 ± 12
700	-1.2 ± 11	0.8 ± 13	2.7 ± 16	8.3 ± 15	5.0 ± 12	-2.3 ± 10
800	-1.2 ± 11	1.6 ± 13	2.1 ± 18	6.8 ± 15	3.2 ± 12	-0.3 ± 9.
900	-1.4 ± 11	2.9 ± 15	1.6 ± 18	5.0 ± 15	1.5 ± 11	0.5 ± 9.
1000	-2.4 ± 11	2.6 ± 16	0.4 ± 18	3.4 ± 15	-0.9 ± 11	-0.2 ± 11
1200	-4.0 ± 10	-1.8 ± 18	-0.1 ± 16	1.7 ± 14	-3.8 ± 10	-2.7 ± 11
1500	-7.7 ± 10	-5.9 ± 17	-1.8 ± 14	-1.9 ± 15	-5.5 ± 12	-5.1 ± 10
2000	-11.4 ± 9.	-11.0 ± 15	-4.7 ± 13	-2.4 ± 16	-8.3 ± 12	-9.0 ± 11
2500	-15.1 ± 11	-15.3 ± 12	-7.2 ± 15	-4.0 ± 15	-13.5 ± 14	-13.0 ± 12
3000	-17.7 ± 11	-18.4 ± 12	-9.7 ± 14	-7.9 ± 17	-17.4 ± 14	-17.0 ± 12

large pollution sources, and so see large variability in surface ozone depending on local winds, insolation and temperature inversions, rendering forecasting more difficult. In Tables 2-6 the standard deviations of the model-sonde differences for these sites decline markedly from the surface to 3000m. Some of the sites near the ocean (Narragansett, RHBrown) appear also to be subject to daylight titration under certain conditions (temperature inversions, clouds or fog). A dramatic example of this was observed at Narragansett on July 28th. Interesting, three of the model runs (AURAMS-NEW, CHRONOS-OP and CHRONOS-SDA) appear to reproduce this, although the predicted loss is only half that observed.

The AURAMS-RT and AURAMS-BIO runs show much larger (negative) biases than the two CHRONOS runs and the AURAMS-NEW run above about 1500 m. As noted above, all of the models show exclusively negative biases above 2000 m.

Another aspect of model performance, one that is perhaps the most important for an AQ *forecast* model, is how well the model predicts changes in ozone concentration from day to day. Several of the IONS sites lauched sondes on a daily or near-daily schedule. Figure 8 shows time series of surface ozone from the ozonesondes at six of these sites, compared with the five model runs. Although individual differences are often significant, all the models track major changes in ozone concentration well overall. Variability in the model values is somewhat higher than in the measured values, by 12% , 32%, 38%, 27% and 17%, for AURAMS-RT, AURAMS-BIO, AURAMS-NEW, CHRONOS-OP and CHRONOS-SDA respectively. Figure 9 is similar, comparing time series of measured ozone at 1000 m with those forecast by the five model versions for the same six sites. All of the models also track major changes in ozone concentration at 1000 m well, although individual differences are often significant. This is

probably in part due to the fact that the models use emissions inventories for ozone precursors, and lack data on actual emisions. For example, none of the model runs predicts the large increases in ozone at 2000m seen over Houston on July 19th and 20th, which were apparently due to pollution from Alaskan and Canadian forest fires [*Morris et al.,* 2006]. Variability in the model values is somewhat higher than in the measured values, by 13%, 34%, 27%, 23%, and 29%, for AURAMS-RT, AURAMS-BIO, AURAMS-NEW, CHRONOS-OP and CHRONOS-SDA, respectively.

3.2 Upper troposphere

In marked contrast to the skill shown in the first 2000 m, above this level all of the models show exclusively negative biases with respect to measurements, and these biases become quite severe, particularly for AURAMS, in the upper troposphere (UT). Figure 10 shows average differences at Egbert, Ontario between the observed and forecast ozone profiles for each model. Other IONS sites show similar differences in the middle and upper troposphere. Possible reasons for this behavior will be discussed in the next section.

4. Discussion

4.1 Intra-version differences

Inspection of Figures 2 to 7 suggests some systematic differences between the five model versions. For example, comparing CHRONOS-OP with CHRONOS-SDA, it is evident from these figures that the addition of surface data assimilation of ozone does not always improve the forecast of surface ozone but at the same time the impact of surface data assimilation reaches into the free troposphere. However, as noted above, a comparison of Tables 5 and 6 suggests slightly better statistics for CHRONOS-SDA. Turning to the AURAMS-RT/AURAMS-BIO

pair, the higher isoprene emissions in the AURAMS-BIO run have resulted in higher mean ozone concentrations at all sites, although the magnitude varies from site to site (Table 2 vs. Table 3). And the profiles from the AURAMS-NEW run presented in Figure 2 to 7 are quite distinct from those of the other two AURAMS runs. The underprediction at upper levels is also significantly reduced for this run, compared to the other two AURAMS runs (e.g., Table 3 vs. Table 4) but is generally still larger than the two CHRONOS runs (e.g., Table 4 vs. Table 5).

It is also instructive to compare the ensemble of the five model-predicted ozone profiles to the measured profile in Figures 2 to 7. In most cases the ensemble of profiles brackets the measured profile, suggesting that an ensemble-average profile might compare better to measurements than any individual model version. Based on the forecasts submitted for the ICARTT real-time AQ model intercomparison, including the CHRONOS-OP and AURAMS-RT forecasts, *McKeen et al*. [2005] and *Pagowski et al*. [2005] found that an ensemble forecast from the six participating AQ model performed better on average than any of the individual models. It is also worth noting given the range of forecasts from basically similar model versions how sensitive model performance can be to changes in model configuration or input files.

4.2 Role of chemical initial and boundary conditions

As discussed by *Brost* [1988], the treatment of moderately long-lived trace species such as ozone poses a challenge for limited-area CTMs, since species whose chemical lifetimes are on the order of days will be long-lived enough to travel from the model boundary to the interior but reactive enough to be transformed or removed within the model domain. This suggests that ozone concentrations at inflow boundaries will influence ozone concentrations in the model interior. As shown by *Brost* [1988] and *Langmann and Bauer* [2002], lateral-boundary influences will

also increase with height, since most emissions of ozone precursors are emitted at or near the Earth's surface and hence have the most immediate impact close to the ground. Thus lateral-boundary influences will be more important in the free troposphere than the PBL. *Lin et al.* [1996] found similar results for Rn-222, an inert gas which has an e-folding lifetime of 5.5 days and only surface sources.

Brost [1988] and *Berge et al.* [2001] have also demonstrated that regional-scale CTMs can be significantly influenced by initial vertical distributions of ozone for three days or more after the start of a simulation before horizontal winds have had time to "flush" the model interior. They also found the influence of initial ozone concentrations to be larger in the free troposphere than the PBL. This phenomenon will be enhanced for the two models considered in this study as they employ a zero-gradient boundary condition for each chemical species at inflow lateral boundaries, and thus in essence ignore inward fluxes at the lateral boundaries.

It is apparent from the model evaluation results presented in Section 3 that model performance was better in the PBL than the free troposphere. This is consistent with the greater role of local emissions of ozone precursors in the former. However, even for the PBL, initial and boundary conditions are likely to have a greater influence for periods when emissions are reduced or transport is from an unpolluted area or photochemistry is reduced (e.g., winter).

The large differences between the AURAMS and CHRONOS deficiencies in the UT are surprising, since, as noted above, the models have many features in common, including the same gas-phase chemistry and the same emissions inventory. Although the two models employ the same chemical lateral boundary conditions, there is a difference in the initial ozone fields.

AURAMS assumes an initial profile of … But other factors may contribute as well. For example, the difference in biogenic emissions between the AURAMS-OP and AURAMS-BIO runs results in somewhat smaller biases in the UT for the latter run. And possible candidates for the even smaller biases for the AURAMS-NEW run are the change in the anthropogenic emission files, the change in the meteorological input files, and the addition of CO as a prognostic species to the gas-phase chemistry mechanism.

4.3 Role of stratosphere-troposphere exchange

There are also several processes not represented in the models that likely contribute to the significant underestimate of ozone in the UT. Emissions of NOx in the UT due to lightning and to in-flight aircraft emissions have not been considered. Such emissions could lead to *in situ* production of ozone. Vertical transport of ozone and its precursors from the PBL to the UT by subgrid-scale deep convective systems such as large thunderstorms or squall lines is also not considered. But the stratosphere is a large reservoir of ozone, and so another potential source of the "missing" ozone is injection from the stratosphere, which is also not presently considered in AURAMS or CHRONOS.

Observational studies on stratosphere-troposphere exchange of ozone comprise a large literature [e.g., *Danielsen*, 1968; *Davies and Schuepbach*, 1994; *Cho et al.,* 1999; *Monks*, 2000]. A number of these studies have suggested that the process is quite important to the tropospheric ozone budget [e.g., *Dutkiewicz and Husain,* 1985; *Oltmans et al.,* 1989; *Bachmeier et al.,* 1994; *Browell et al.,* 1994; *Mauzerall et al.,* 1996; *Dibb et al.,* 1997; 2003; *Allen et al.,* 2003], while others have concluded that it is a minor source [e.g., *Dibb et al.,* 1994; *Bazhanov and Rodhe*, 1997; *Elbern et al.,* 1997; *Li et al.,* 2002; *Browell et al.,* 2003]. In general, the former studies

dealt with the UT while the latter concluded that stratospheric ozone was a minor source at the surface. Other ozonesonde-model comparison studies [*Hoff et al.,* 1995; *Mauzerall et al.,* 1996] have found it necessary to assume a stratospheric ozone source in order to reproduce the observed vertical distribution of ozone. Indeed, consideration of the average vertical profile of ozone molar mixing ratio at any of the IONS sites (e.g., Figure 11) strongly suggests that the stratosphere must be a source of at least some of the ozone in the troposphere, since the observed monotonic decline of ozone mixing ratio from the tropopause to the PBL cannot readily be explained by means of only tropospheric sources.

Estimates by global CTMs of the cross-tropopause flux of ozone from the stratosphere vary between about 400 and 1400 $Tg(O_3)\ yr^{-1}$ [*WMO*, 1999; *Brasseur et al.,* 2003]. More recently *Lelieveld and Dentener* [2000] have estimated it to be 565 $Tg(O_3)\ yr^{-1}$, based on a model study using ECMWF meteorological reanalyses and ozonesonde data. The flux has also been estimated from measurements of N_2O and ozone, based on the observed correlation of N_2O and ozone, at 400 $Tg(O_3)\ yr^{-1}$ [*Murphy and Fahey* , 1994], and at 475 $Tg(O_3)\ yr^{-1}$ [*McLinden et al.,* 2000], from measurements of N_2O and NO_y, based on the observed correlation between N_2O and NO_y. These fluxes are comparable to the total tropospheric burden of ~350 $Tg(O_3)$.

It is a fairly simple matter to estimate the rate of transport of ozone from the stratosphere that would be necessary to account for the "missing" ozone in Figure 10, for example. The vertical ozone flux f through a horizontal surface can be written

$$f = -K\rho\frac{d\mu}{dz} \qquad (1)$$

where $\mu=\rho_{O_3}/\rho$ is the ozone mass mixing ratio, ρ is air density and z is the vertical coordinate. Then assuming no *in situ* production or loss, the change in ozone concentration within a horizontal layer is given by the difference in vertical flux at the top and bottom surfaces, divided by the layer thickness:

$$\rho\frac{d\mu}{dt}=\frac{flux_{top}-flux_{bottom}}{z_{top}-z_{bottom}}=\frac{df}{dz} \tag{2}$$

or

$$\frac{d\mu}{dt}=\rho^{-1}\frac{d}{dz}(-K\rho\frac{d\mu}{dz}) \tag{3}$$

This will be recognized as the equation for diffusion of μ in one dimension. K (often written K_{zz}) is the coefficient of vertical diffusion and has a value appropriate to represent all vertical motion in the atmosphere (as opposed to the K described in a three-dimensional atmospheric model like GEM, which represents only turbulent eddy diffusion, since large-scale vertical motions in GEM are modeled explicitly).

For a steady state, the left-hand side of (3) must be balanced by an equal rate of chemical loss. We assume a chemical loss rate, L = 2 ppb/day. This corresponds to a lifetime for ozone at the surface of about two weeks, and 40 days in the UT. We scale this assumed total L by the fraction of "missing" ozone and set it equal to the flux divergence, $d\mu/dt$, above. From the sonde data, we know ρ and $d\mu/dz$, and so can solve for the value of K that is required (for the assumed rate of chemical loss) in order to supply the missing ozone by downward transport. From (1) we can

then calculate the flux of ozone from the model top (or the tropopause) that is implied by this. Figure 12 shows the result of this calculation for Yarmouth, Nova Scotia, using an average of sonde data over several stations for $d\mu/dz$.

It is difficult to estimate the range of values for *K* that might be expected, since *K* is neither a real (i.e., measurable) atmospheric variable nor is it expressed in global 3D models like GEM. However, values of *K* used in 1D and 2D models are generally in the range 4-10 $m^2 s^{-1}$ [*Mauzerall et al.,* 1996; *IPCC,* 1999]. From Figure 12 one can see that the *K* profile that we estimate for this site is ~30 $m^2 s^{-1}$ or less; for other IONS sites it is quite similar. Figure 12 also indicates the fluxes of ozone from the upper boundaries (or tropopause) of the models that is implied: for this site they fall in the range 800-3000 $Tg(O_3) yr^{-1}$. Again, for other IONS sites the range is similar. Note that only the larger values are actually cross-tropopause fluxes; for the three model versions with lids below the tropopause the calculated fluxes need to be extrapolated to 10 km (the assumed average height of the tropopause) to be strictly comparable.

Compared to the other estimates quoted above, these values for *K* and the cross-tropopause flux appear somewhat high, particularly for AURAMS. However, we note that they should be regarded as order-of-magnitude estimates only, since both the *K* and *f* values we derive by this calculation are proportional to the assumed chemical destruction rate, *L*. Had we assumed a longer lifetime for ozone in the UT, e.g. *L* = 1 ppb/day, then we would have derived values half as large for both *K* and *f*. It seems quite possible, therefore, that the addition of a realistic stratosphere, and the corresponding stratospheric ozone flux, would significantly improve the model profiles of ozone in the UT. However, unless the ozone lifetime there is much longer than we have assumed, it seems likely that some additional chemical source of ozone in the UT will

also be required. One likely candidate is lightning-generated NO_x [*Huntrieser et al.*, 1998; *Cooper et al*., 2006], which is not currently considered in either model.

It is reasonable to ask whether or not correcting the profile in the free troposphere would have an important effect on modeled ozone values at the surface. Stratospheric ozone intrusions are occasionally observed to reach the ground [e.g. *Lefohn et al.,* 2001; *Elbern et al.,* 1997; *Davies and Schuepbach*, 1994; *Wakamatsu et al.,* 1989; *Oltmans et al.,* 1989], so the addition of a stratospheric source would clearly improve modeling of these events; however, they are relatively infrequent. Much more frequently, intrusion events are observed to reach the upper or middle troposphere, where they appear to dissipate and contribute to the "background" ozone, generally defined as tropospheric ozone that is more than seven days old and therefore of uncertain origin, and estimated at about 20-45 ppb [*Naja et al.,* 2003; *Altshuller and Lefohn*, 1996; *Hirsch et al.*, 1996; *Lin et al.*, 2000]. Since the troposphere is generally well-mixed on a time scale of two to three weeks, and the lifetime of ozone in the lower troposphere is of similar duration, this background ozone likely makes a significant, seasonally varying contribution to ozone values at the surface. Indeed, long-term trend studies of ozonesonde data find statistically significant (95% confidence) correlations between ozone mixing ratio in the lower stratosphere and in the troposphere, right down to the surface, at mid- and high latitude sites far from major anthropogenic pollution sources [*Tarasick et al*., 2005; *Taalas et al*., 1997]. The fact that all the models overpredict the variance of ozone in the surface layer (Figures 8 and 9) is consistent with such a background contribution, since if they lack a (constant) background term they may overpredict chemical production in order to compensate. Further evidence that ozone from the free troposphere affects the surface is found in the observed diurnal cycle of ozone at most urban

sites; the ozone that is destroyed by NO titration is replenished each day when the nighttime surface inversion is dispersed in the morning and ozone is mixed down from the residual layer.

5. Conclusions

The availability of the IONS-04 data set, which consists of a sizable number of quasi-daily ozone vertical profiles at 12 sites in North America during a five-week period in summer 2004, constitutes a valuable new resource for evaluating the performance of complex regional chemical transport models above the surface. Two such models, AURAMS and CHRONOS, both show considerable skill at forecasting boundary-layer ozone but have serious discrepancies in the free troposphere on average when compared to the IONS-04 profiles. These findings would not have been attainable from model evaluations based only on surface observations, which is all that is usually available to modelers, and they help to identify areas of individual models that require further work. For example, the analysis presented here suggests that significant improvement in model performance in the free troposphere may be obtained by adding a realistic stratospheric ozone flux term. Work is now in progress to develop a version of GEM with in-line chemistry, which will also carry a stratospheric ozone tracer. This should improve the skill of the air quality forecast system.

Acknowledgements

Thanks are due to B. Pabla, M. Sassi, S. Gaudreault, and J. Zhang of Environment Canada for their assistance in developing and running AURAMS and to D. Dégardin of the University of Quebec at Montreal for his work on the AURAMS-BIO simulation. The provision of a set of

evaluations of CHRONOS and AURAMS performance during the ICARTT period by S. McKeen of NOAA in Boulder, Colorado, was much appreciated.

References

Altshuller, A. P., and A. S. Lefohn (1996), Background ozone in the planetary boundary layer over the United States, *J. Air Waste Manage. Assoc.*, *46*, 134–141.

Bachmeier, E.V., M.C. Shipman, E.V. Browell, W.B. Grant, and J.M. Klassa (1994), Stratospheric/tropospheric exchange affecting the northern wetlands regions of Canada during summer 1990, *J. Geophys. Res., 99*, 1793-1804.

Bazhanov, V. and H. Rodhe (1997), Tropospheric ozone at the Swedish mountain site Åreskutan: Budget and trends, *J. Atmos. Chem.*, *28*, 61-76.

Berge, E., H.-C. Huang, J. Chang, and T.-H. Liu (2001), A study of the importance of initial conditions for photochemical oxidant modeling, *J. Geophys. Res*., *106 (D1)*, 1347-1363.

Brasseur, G.P., R.G. Prinn, and A.A.P. Pszenny, (eds.) (2003), *Atmospheric Chemistry in a Changing World. An Integration and Synthesis of a Decade of Tropospheric Chemistry Research***.** The International Global Atmospheric Chemistry Project of the International Geosphere-Biosphere Programme. – Springer-Verlag, Berlin .

Brost, R.A. (1988), The sensitivity to input parameters of atmospheric concentrations simulated by a regional chemical model. *J. Geophys. Res., 93(D3)*, 2371-2387.

Browell, E.V., M.A. Fenn, C.F. Butler, W.B. Grant, R.C. Harriss, and M.C. Shipman (1994), Ozone and aerosol distributions in the summertime troposphere over Canada, *J. Geophys. Res., 99*, 1739-1755.

Browell, E.V., et al. (2003), Ozone, aerosol, potential vorticity, and trace gas trends observed at high-latitudes over North America from February to May 2000, *J. Geophys. Res., 108*(*D4)*, 8369, doi:10.1029/2001JD001390.

Carolina Environmental Program (2006), http://cf.unc.edu/cep/empd/products/smoke/index.cfm (visited 23 June 2006).

Cho, J., et al. (1999), Observations of convective and dynamical instabilities in tropopause folds and their contribution to stratosphere-troposphere exchange, *J. Geophys. Res., 104*, 21,549– 21,568.

Cooper, O.R, A. Stohl, M. Trainer, A. Thompson, J.C. Witte, S.J. Oltmans, G. Morris, K.E. Pickering, J.H. Crawford, Gao Chen, R.C. Cohen, T.H. Bertram, P. Wooldridge, A. Perring, W.H. Brune, J. Merrill, J. L. Moody, D. Tarasick, P. Nédélec, G. Forbes, M. J. Newchurch, F. J. Schmidlin, B. J. Johnson, S. Turquety, S. L. Baughcum, X. Ren, F. C. Fehsenfeld, J. F. Meagher, N. Spichtinger, C.C. Brown, S.A. McKeen, I.S. McDermid, and T. Leblanc (2006), Large upper tropospheric ozone enhancements above mid-latitude North America during summer: In situ evidence from the IONS and MOZAIC ozone measurement network, *J. Geophys. Res.,* In press.

Côté, J., J.-G. Desmarais, S. Gravel, A. Méthot , A. Patoine, M. Roch and A. Staniforth (1998), The operational CMC/MRB Global Environmental Multiscale (GEM) model. Part 1: Design considerations and formulation, *Mon. Wea. Rev.*, *126*, 1373-1395.

Côté, J., J.-G. Desmarais, S. Gravel, A. Méthot, A. Patoine, M. Roch, and A. Staniforth (1998b) The operational CMC-MRB Global Environment Multiscale (GEM) model. Part II: Results. *Mon. Wea. Rev.*, *126,* 1397-1418.

Danielsen, E. F. (1968), Stratospheric-tropospheric exchange based upon radioactivity, ozone, and potential vorticity, *J. Atmos. Sci., 25*, 502–518.

Davies, T.D. and Schuepbach, E. (1994), Episodes of high ozone concentrations at the Earth's surface resulting from transport down from the upper troposphere/lower stratosphere: A review and case studies, *Atmospheric Environment*, *28*, No.1,53-68.

Dibb, J. E., L. D. Meeker, R. C. Finkel, J. R. Southon, M. W. Caffee, and L. A. Barrie (1994), Estimation of stratospheric input to the Arctic troposphere: ^{7}Be and ^{10}Be aerosols at Alert, Canada, *J. Geophys. Res., 99*, 12,855–12,864.

Dibb, J. E., R. W. Talbot, B. L. Lefer, E. Scheuer, G. L. Gregory, E. V. Browell, J. D. Bradshaw, S. T. Sandholm, and H. B. Singh (1997), Distributions of beryllium 7 and lead 210, and soluble aerosol-associated ionic species over the western Pacific: PEM West B, February–March 1994, *J. Geophys. Res., 102*, 28,287– 28,302.

Dibb, J. E., R. W. Talbot, E. Scheuer, G. Seid, L. DeBell, B. L. Lefer, and B. Ridley (2003), Stratospheric influence on the northern North American free troposphere during TOPSE: ^{7}Be as a stratospheric tracer, *J. Geophys. Res., 108*(D4), 8363, doi:10.1029/2001JD001347.

Dutkiewicz, V. A., and L. Husain (1985), Stratospheric and tropospheric components of ^{7}Be in surface air, *J. Geophys. Res., 90*, 5783–5788.

Elbern, H., Kowol, J., Sladkovic, R., and Ebel, A. (1997), Deep stratospheric intrusions: A statistical assessment with model guided analysis, *Atmospheric Environment*, *31*, No. 19, 3207-3226.

Frost G.J., S.A. McKeen, M. Trainer, T.B. Ryerson, J.A. Neuman, J.M. Roberts, A. Swanson, J.S. Holloway, D.T. Sueper, T. Fortin, D.D. Parrish, F.C. Fehsenfeld, F. Flocke, S.E. Peckham, G. A. Grell, D. Kowal, J. Cartwright, N. Auerbach, and T. Habermann (2006), Effects of changing power plant NO_x emissions on ozone in the eastern United States: Proof of concept, *J. Geophys. Res., 111*, D12306, doi:10.1029/2005JD006354.

Gong, S.L., L.A. Barrie, J.-P. Blanchet, K. von Salzen, U. Lohmann, G. Lesins, L. Spacek, L.M. Zhang, E. Girard, H. Lin, R. Leaitch, H. Leighton, P. Chylek, and P. Huang (2003a), Canadian Aerosol

Module: A size segregated simulation of atmospheric aerosol processes for climate and air quality models: Part 1. Module development. *J. Geophys. Res., 108*(D1), 4007, doi:10.1029/2001JD002002, 16 pp.

Gong, W., P.A. Makar, and M.D. Moran (2003b), "Mass-conservation issues in modelling regional aerosols". *Proc. 26th NATO/CCMS ITM on Air Pollution Modelling and Its Application*, May 26-29, Istanbul, Turkey. [In *Air Pollution Modelling and Its Application XVI*, C. Borrego and S. Incecik, Editors, Kluwer/Plenum Publishers, New York, 383-391.]

Gong, W., A.P. Dastoor, V.S. Bouchet, S. Gong, P.A. Makar, M.D. Moran, B. Pabla, S. Ménard, L-P. Crevier, S. Cousineau, and S. Venkatesh (2006), Cloud processing of gases and aerosols in a regional air quality model (AURAMS), *Atmos. Res*. (Accepted).

Hirsch, A. I., J. W. Munger, D. J. Jacob, L. W. Horowitz, and A. H. Goldstein (1996), Seasonal variation of the ozone production efficiency per unit NOx at Harvard Forest, Massachusetts, *J. Geophys. Res.*, *101*, 12,659–12,666.

Hoff, R. M., R. E. Mickle and C. Fung (1995), Vertical profiles of ozone during the EMEFS I experiment in southern Ontario, *Atmos. Environ*., *29*, 1735-1747.

Houyoux, M.R., Vukovich, J.M., Coats, Jr., C.J. and Wheeler, N.J.M (2000), Emission inventory development and processing for the Seasonal Model for Regional Air Quality (SMRAQ) project, *J. Geophys. Res., 105*, 9079-9090.

Huntrieser, H., H. Schlager, C. Feigl, H. Höller (1998), Transport and production of NO_x in electrified thunderstorms: Survey of previous studies and new observations at midlatitudes, *J. Geophys. Res., 103*(D21), 28247-28264, 10.1029/98JD02353,.

IPCC Special Report (1999), *Aviation and the Global Atmosphere*, edited by J.E. Penner, D.H. Lister, D.J. Griggs, D.J. Dokken, and M. McFarland, Intergovernmental Panel on Climate Change, Cambridge Press, Cambridge.

Isaksen, I.S.A., C. Zerefos, K. Kourtidis, C. Meleti, S. B. Dalsøren, J.K. Sundet, A. Grini, P. Zanis, and D. Balis (2005), Tropospheric ozone changes at unpolluted and semipolluted regions induced by stratospheric ozone changes, *J . Geophys. Res., 110*, D02302, doi:10.1029/2004JD004618.

Jiang, W. (2003), Instantaneous secondary organic aerosol yields and their comparison with overall aerosol yields for aromatic and biogenic hydrocarbons, *Atmos. Environ., 37*, 5439-5444.

Kerr, J.B., H. Fast, C.T. McElroy, S.J. Oltmans, J.A. Lathrop, E. Kyro, A. Paukkunen, H. Claude, U. Köhler, C.R. Sreedharan, T. Takao and Y. Tsukagoshi (1994), The 1991 WMO international ozonesonde intercomparison at Vanscoy, Canada,. *Atmosphere-Ocean, 32*, 685-716,.

Kinnee, E., C. Geron, and T. Pierce (2005), Development of a 1-km resolved vegetation database for surface exchange modeling in North America, *Ecol. Appl.*, in press.

Langmann, B. and S.E. Bauer (2002), On the importance of reliable background concentrations of ozone for regional scale photochemical modelling. *J. Atmos. Chem.*, **42**, 71-90.

Lefohn, A. S., Oltmans, S. J., Dann, T. and Singh, H. B. (2001), Present-day variability of background ozone in the lower troposphere. *J. Geophys. Res.*, *106(*D9), 9945–9958.

Lelieveld, J., and F. J. Dentener (2000), What controls tropospheric ozone?, *J. Geophys. Res.*, *105*(D3), 3531–3552.

Li, Q., D. J. Jacob, T. D. Fairlie, H. Liu, R. V. Martin, and R. M. Yantosca (2002), Stratospheric versus pollution influences on ozone at Bermuda: Reconciling past analyses, *J. Geophys. Res., 107*(D22), 4611, doi:10.1029/2002JD002138.

Lin, X., F. Zaucker, E.-Y. Hsie, M. Trainer, and S.A. McKeen (1996), Radon 222 simulations as a test of a three-dimensional regional transport model, *J. Geophys. Res., 101(D22)*, 29,165-29,177.

Lin, C.-Y. C., D. J. Jacob, J. W. Munger, and A. M. Fiore (2000), Increasing background ozone in surface air over the United States, *Geophys. Res. Lett.*, *27*, 3465–3468.

Makar, P.A., V.S. Bouchet, and A. Nenes(2003a), Inorganic chemistry calculations using HETV˜ a vectorized solver for the SO42˜-NO3˜-NH4+ system based on the ISORROPIA algorithms, *Atmos. Environ*., *37***,** 2279-2294.

Makar, P.A., M.D. Moran, M.T. Scholtz and A. Taylor (2003b), Speciation of volatile organic compound emissions for regional air quality modelling of particulate matter and ozone, *J. Geophys. Res., 108 (D2)*, 4041, doi:10.1029/2001JD000797, 51 pp.

Makar, P.A. et al. (2006).

Mauzerall, D.L.**,** Jacob, D.J., Fan, S.M., Bradshaw, J.D., Gregory, G.L., Sachse, G.W. and D. R. Blake (1996), Origins of tropospheric ozone at remote high northern latitudes in summer, *J. Geophys. Res.*, *101*, 4175-4188.

McKeen, S.A. (2005), Personal communication.

McKeen, S., J. Wilczak, G. Grell, I. Djalalova, S. Peckham, E.-Y. Hsie, W. Gong, V. Bouchet, S. Ménard, R. Moffet, J. McHenry, J. McQueen, Y. Tang, G.R. Carmichael, M. Pagowski, A. Chan, and T. Dye (2005), Assessment of an ensemble of seven real-time ozone forecasts over Eastern North America during the summer of 2004, *J. Geophys. Res., 110*, D21307, doi:10.1029/2005JD005858.

McLinden, C., S. Olsen, B. Hannegan, O. Wild, M. Prather, and J. Sundet (2000), Stratospheric ozone in 3-D models: A simple chemistry and the cross-tropopause flux, *J. Geophys. Res., 105*, 14653-14665.

Monks, P.S. (2000), A review of observations and origins of the spring ozone maximum, *Atmos. Environ.*, *34*(21), 3545-3561.

Morris, G.A., S. Hersey, A.M. Thompson, O.R. Cooper, A. Stohl, P.R. Colarco, W.W. McMillan, J. Warner, B.J. Johnson, J.C. Witte, T.L. Kucsera, D.E. Larko, and S.J. Oltmans, Alaskan and Canadian forest fires exacerbate ozone pollution over Houston, Texas, on 19 and 20 July 2004, *J. Geophys. Res.*, 10.1029/2006JD007090, in press, 2006.

Murphy, D. M., and D. W. Fahey (1994), An estimate of the flux of stratospheric reactive nitrogen and ozone into the troposphere, *J. Geophys. Res.*, *99*(D3), 5325–5332.

Naja M., H. Akimoto, and J. Staehelin (2003), Ozone in background and photochemically aged air over central Europe: Analysis of long-term ozonesonde data from Hohenpeissenberg and Payerne, *J. Geophys. Res., 108* (D2), 4063, doi:10.1029/2002JD002477.

Odum, J.R., T. Hoffman, F. Bowman, D. Collins, R.C. Flagan, and J.H. Seinfeld (1996), Gas/particle partitioning and secondary aerosol formation, *Environ. Sci. Technol*., *30*, 2580-2585.

Oltmans, S.J., W.E. Raatz and W.D. Komhyr (1989), On the transfer of stratospheric ozone into the troposphere near the north pole, *J. Atmos. Chem., 9*, 245--253.

Pagowski, M., G.A. Grell, S.A. McKeen, D. Dévényi, J.M. Wilczak, V. Bouchet, W. Gong, J. McHenry, S. Peckham, J. McQueen, R. Moffet, and Y. Tang (2005), A simple method to improve ensemble-based ozone forecasts, *Geophys. Res. Let., 32*, L07814, doi:10.1029/2004GL022305, 4 pp.

Pandis, S.N., R.A. Harley, G.R. Cass, and J.H. Seinfeld (1992), Secondary organic aerosol formation and transport. *Atmos. Environ., 26A*, 2269-2282.

Pierce, T. C. Geron, L. Bender, R. Dennis, G. Tonnesen, and A. Guenther (1998), The influence of increased isoprene emissions on regional ozone modeling, *J. Geophys. Res., 103*, 25,611-25,629.

Pudykiewicz, J.A., A. Kallaur, and P.K. Smolarkiewicz (1997), Semi-Lagrangian modelling of tropospheric ozone, *Tellus*, *49B*, 231-248.

Scholtz, M.T., A. Taylor, A. Ivanoff, M.D. Moran, D. Davies, P.A. Makar, S. Venkatesh, P. Cheung and J. Barton (1999), Application of the Canadian Emissions Processing System, Version 1.0 (CEPS1.0): four case studies, *Proc. 9th AWMA Emission Inventory Symp*., AWMA Book VIP-93, Oct. 26-28, Raleigh, North Carolina, Air & Waste Management Association, Pittsburgh, 456-468.

Sirois, A., J.A. Pudykiewicz, and A. Kallaur (1999), A comparison between simulated and observed ozone mixing ratios in eastern North America, *J. Geophys. Res.*, *104*, 21,397-21,423.

Smit, H.G.J., W. Straeter, B. Johnson, S. Oltmans, J. Davies, D.W. Tarasick, B. Hoegger, R. Stubi, F. Schmidlin, T. Northam, A. Thompson, J. Witte, I. Boyd and F. Posny (2006), Assessment of the performance of ECC-ozonesondes under quasi-flight conditions in the environmental simulation chamber: Insights from the Jülich Ozone Sonde Intercomparison Experiment (JOSIE), submitted to *JGR*.

Taalas, P., J. Damski, E. Kyrö, M. Ginzburg, G. Talamoni (1997), Effect of stratospheric ozone variations on UV radiation and on tropospheric ozone at high latitudes, *J. Geophys. Res*., *102*(D1), 1533-1540, 10.1029/96JD02310.

Tarasick, D.W., V.E. Fioletov, D.I. Wardle, J.B. Kerr and J. Davies (2005) Changes in the vertical distribution of ozone over Canada from ozonesondes: 1980-2001, *J. Geophys. Res., 110*, D02304, doi:10.1029/2004JD004643.

Thompson, A.M., J.B. Stone, J.C. Witte, R.B. Pierce , R.B. Chatfield, S.J Oltmans, O.R. Cooper, B.F. Taubman, B.J. Johnson, E. Joseph, T.L. Kucsera, J.T. Merrill, G. Morris, S. Hersey, M.J. Newchurch, F.J. Schmidlin, D.W. Tarasick, V. Thouret, J.-P. Cammas (2006), IONS-04 (INTEX Ozonesonde Network Study, 2004): Perspective on summertime UT/LS (upper troposphere/lower stratosphere) ozone over northeastern North America, Submitted to *J. Geophys. Res.* (INTEX Issue) 2006JD007441.

U.S. EPA (2004), *NOx Budget Trading Program: 2003 Progress and Compliance Report*, Clean Air Markets Program, Office of Air and Radiation, U.S. Environmental Protection Agency, Washington, D.C., August, 28 pp. + App. [Available from http://www.epa.gov/airmarkets/fednox/index.html]

U.S. EPA (2001), http://www.epa.gov/asmdnerl/biogen.html (viewed 23 June 2006).

Wakamatsu, S., I. Uno, H. Ueda, K. Uehara, and H. Tateishi (1989), Observational study of stratospheric ozone intrusions into the lower troposphere, *Atmos. Environ., 23,* 1815–1826.

World Climate Research Programme (1998), *SPARC/IOC/GAW Assessment of Trends in the Vertical Distribution of Ozone, Stratospheric Processes and Their Role in Climate, World Meteorol. Organ. Global Ozone Res. Monit. Proj. Rep. 43*, Geneva, Switzerland.

World Meteorological Organization (WMO) (1999), *Scientific Assessment of Ozone Depletion: 1998, Global Ozone Res. Monit. Proj. Rep. 44,* Geneva, Switzerland.

Zhang, L., M.D. Moran, and J.R. Brook (2001), A comparison of models to estimate in-canopy photosynthetically active radiation and their influence on canopy stomatal resistance, *Atmos. Environ*., *35***,** 4463-4470.

Zhang, L., M.D. Moran, P.A. Makar, J.R. Brook and S. Gong (2002), Modelling gaseous dry deposition in AURAMS -- A Unified Regional Air-quality Modelling System, *Atmos. Environ.*, *36*, 537-560.

List of Figures

Figure 1. Location of 12 IONS ozonesonde sounding sites relative to the AURAMS and CHRONOS model domains used in this study. The ozonesonde site numbers correspond to the site list given in Table 1. Note that the Boulder and Trinidad Head sites are outside of the AURAMS domain.

Figure 2. Ozone profile comparisons of the five model runs and the ozonesonde data, for July 14th at Egbert, Ontario. All the models show some skill at reproducing the sharp boundary layer transition in the vertical, and the CHRONOS runs also reproduce the secondary feature at 2km.

Figure 3. Ozone profile comparisons of the five model runs and the ozonesonde data, for July 30th at Sable Island. The boundary layer transition in the vertical is less pronounced for the evening comparison. Two of the AURAMS runs predict this well, but are biased low overall. The CHRONOS runs predict a sharper transition.

Figure 4. Ozone profile comparisons of the five model runs and the ozonesonde data, for July 30th at Yarmouth, Nova Scotia. What appears to be a marine boundary layer transition in the vertical is surprisingly sharp for this late afternoon comparison. Nevertheless, the two CHRONOS runs predict this well.

Figure 5. Ozone profile comparisons of the five model runs and the ozonesonde data, for July 16th at Huntsville, Alabama. All the models predict large ozone production in the surface layer, although underpredicting higher up.

Figure 6. Ozone profile comparisons of the five model runs and the ozonesonde data, for August 10th at Narragansett, Rhode Island. All the models predict large ozone production in the surface layer, although underpredicting higher up. Some of the runs show some indication of the secondary peak at 1 km.

Figure 7. Ozone profile comparisons of the five model runs and the ozonesonde data, for July 7th at Wallops Island, Virginia. Four of the models predict the ozone feature near 1 km. Some of the runs show some indication of the secondary peak at 2 km.

Figure 8. Surface ozone from ozonesondes at six IONS sites compared with the five model runs. Although individual differences are often significant, all the models track major changes in ozone concentration well. Variability in the model values is somewhat higher than in the measured values, by 12% , 32%, 38%, 27% and 17%, for AURAMS-RT, AURAMS-BIO, AURAMS-NEW, CHRONOS-OP and CHRONOS-SDA respectively.

Figure 9. Ozone at 1000m from the five model runs and the ozonesonde data, at six IONS sites. Although individual differences are often significant, all the models track major changes in ozone concentration well. Variability in the model values is somewhat higher than in the measured values, by 13%, 34%, 27%, 23%, and 29%, for AURAMS-RT, AURAMS-BIO, AURAMS-NEW, CHRONOS-OP and CHRONOS-SDA, respectively.

Figure 10. Average differences (model-sonde) between the observed and forecast ozone profiles for each model at Yarmouth, Nova Scotia. Dashed lines indicate 1σ limits. Differences for other sites are similar in the upper troposphere.

Figure 11. Ozone molar mixing ratio from ozonesondes at Egbert, Ontario, averaged on AURAMS model levels. As for other sites, ozone decreases monotonically from the stratosphere to the surface boundary layer.

Figure 12. Calculated values of K_{zz} and cross-tropopause flux necessary to account for the average differences between the observed and forecast ozone profiles shown in Figure 10. Neither AURAMS nor CHRONOS includes a realistic stratosphere (although the AURAMS

model lid was set at 29 km for some of the ICARTT runs, the model did not include stratospheric chemistry or any other source of large ozone mixing ratios in this region).

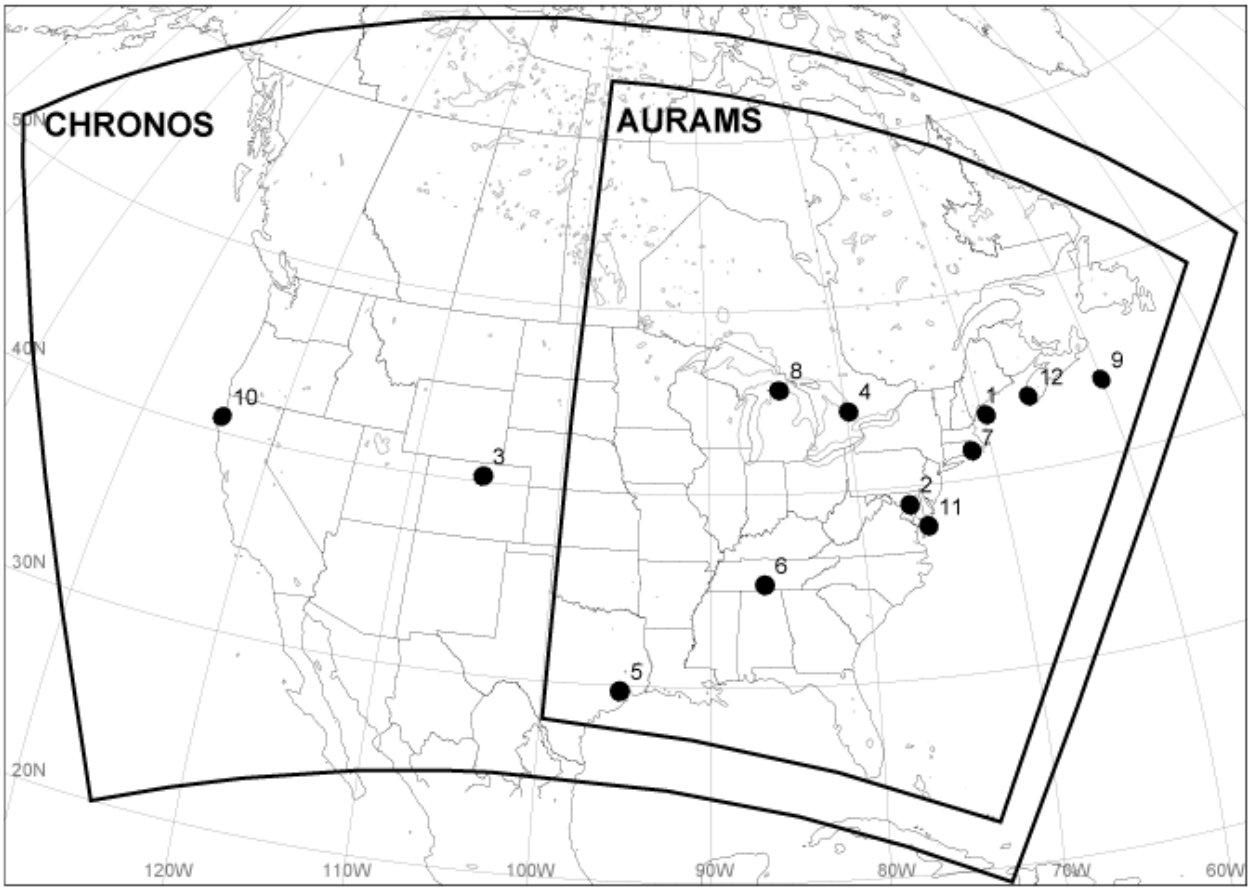

Figure 1. Location of 12 IONS ozonesonde sounding sites relative to the AURAMS and CHRONOS model domains used in this study. The ozonesonde site numbers correspond to the site list given in Table 1. Note that the Boulder and Trinidad Head sites are outside of the AURAMS domain.

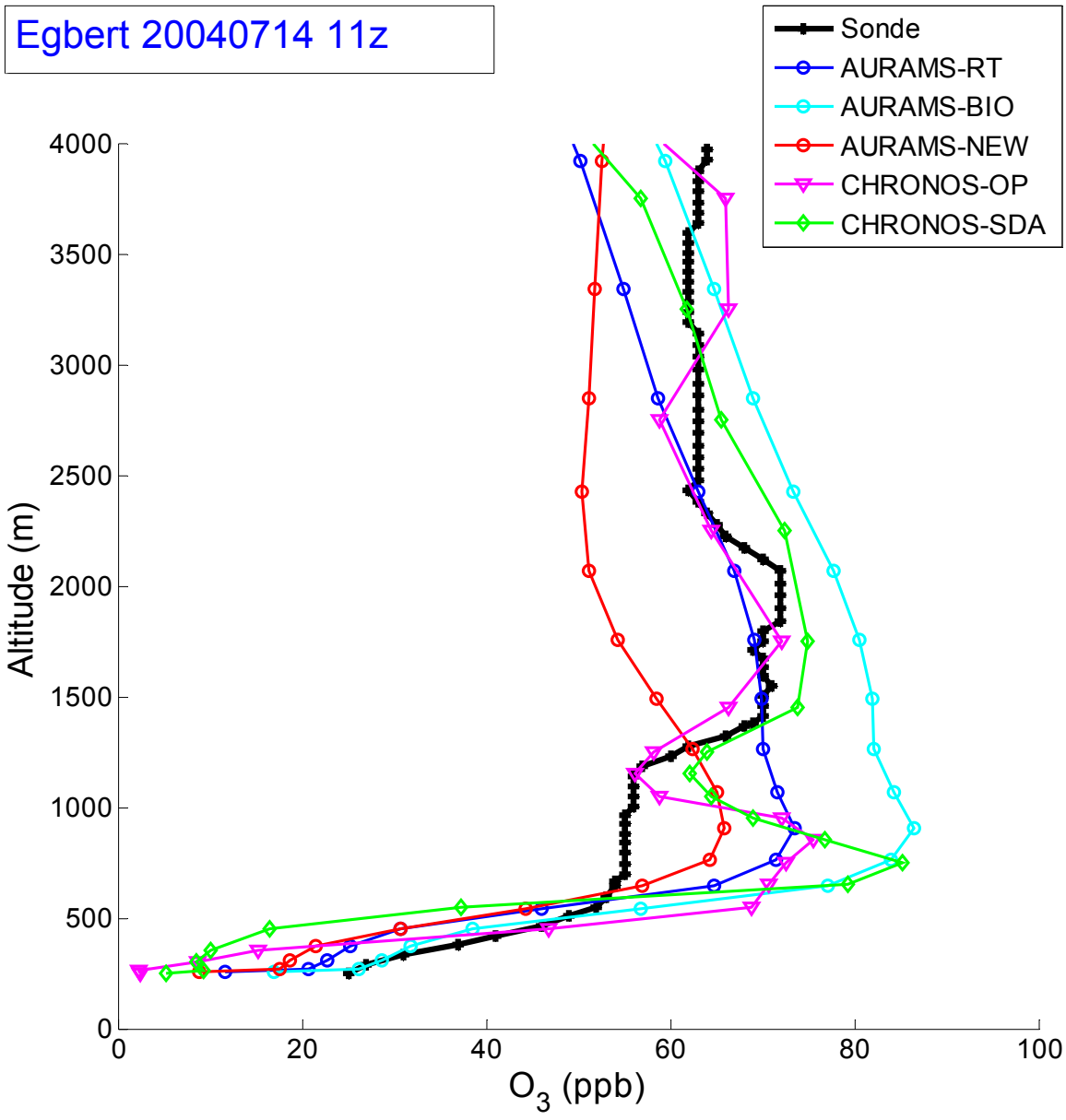

Figure 2. Ozone profile comparisons of the five model runs and the ozonesonde data, for July 14th at Egbert, Ontario. All the models show some skill at reproducing the sharp boundary layer transition in the vertical, and the CHRONOS runs also reproduce the secondary feature at 2km.

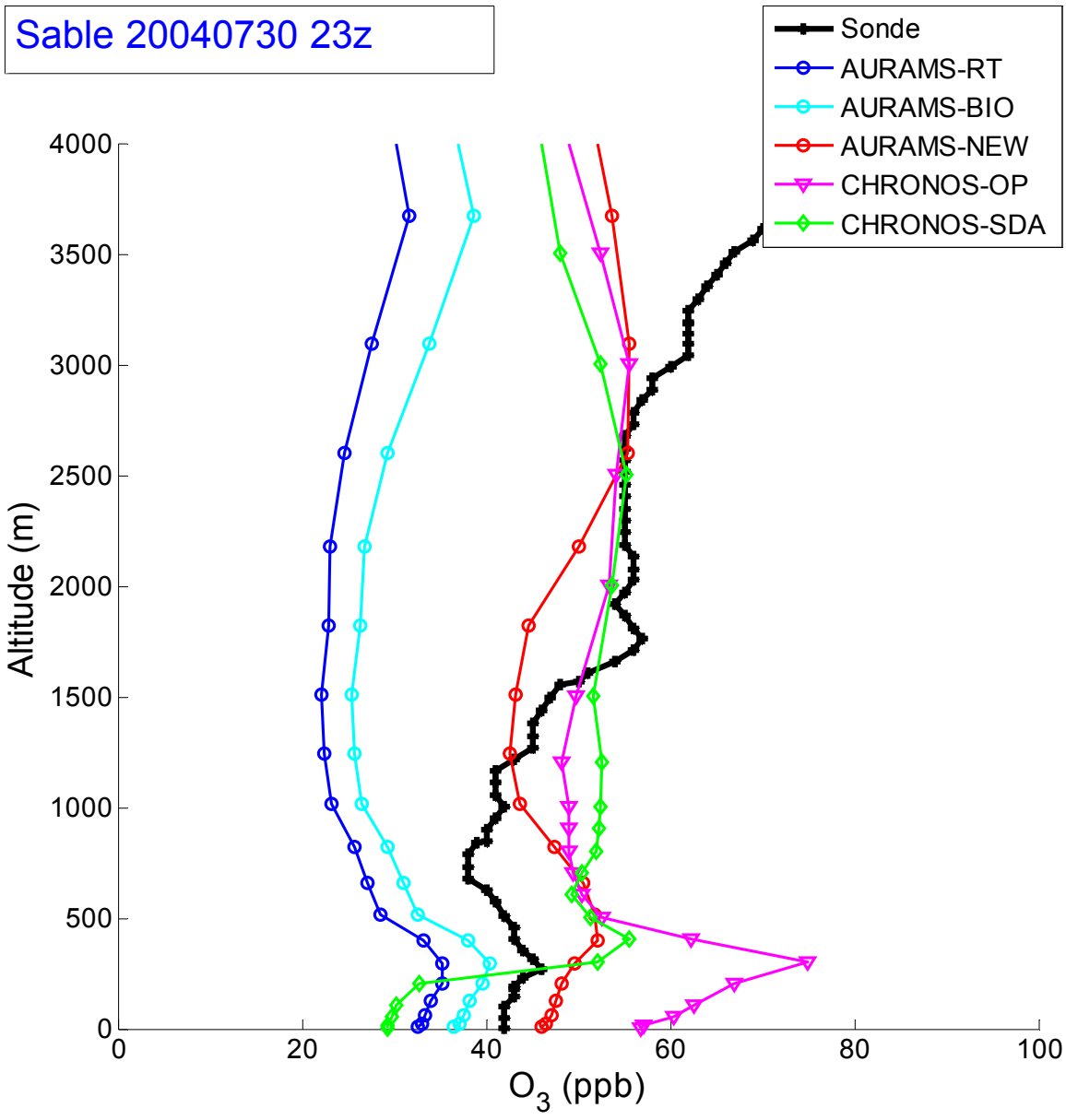

Figure 3. Ozone profile comparisons of the five model runs and the ozonesonde data, for July 30th at Sable Island. The boundary layer transition in the vertical is less pronounced for the evening comparison. Two of the AURAMS runs predict this well, but are biased low overall. The CHRONOS runs predict a sharper transition.

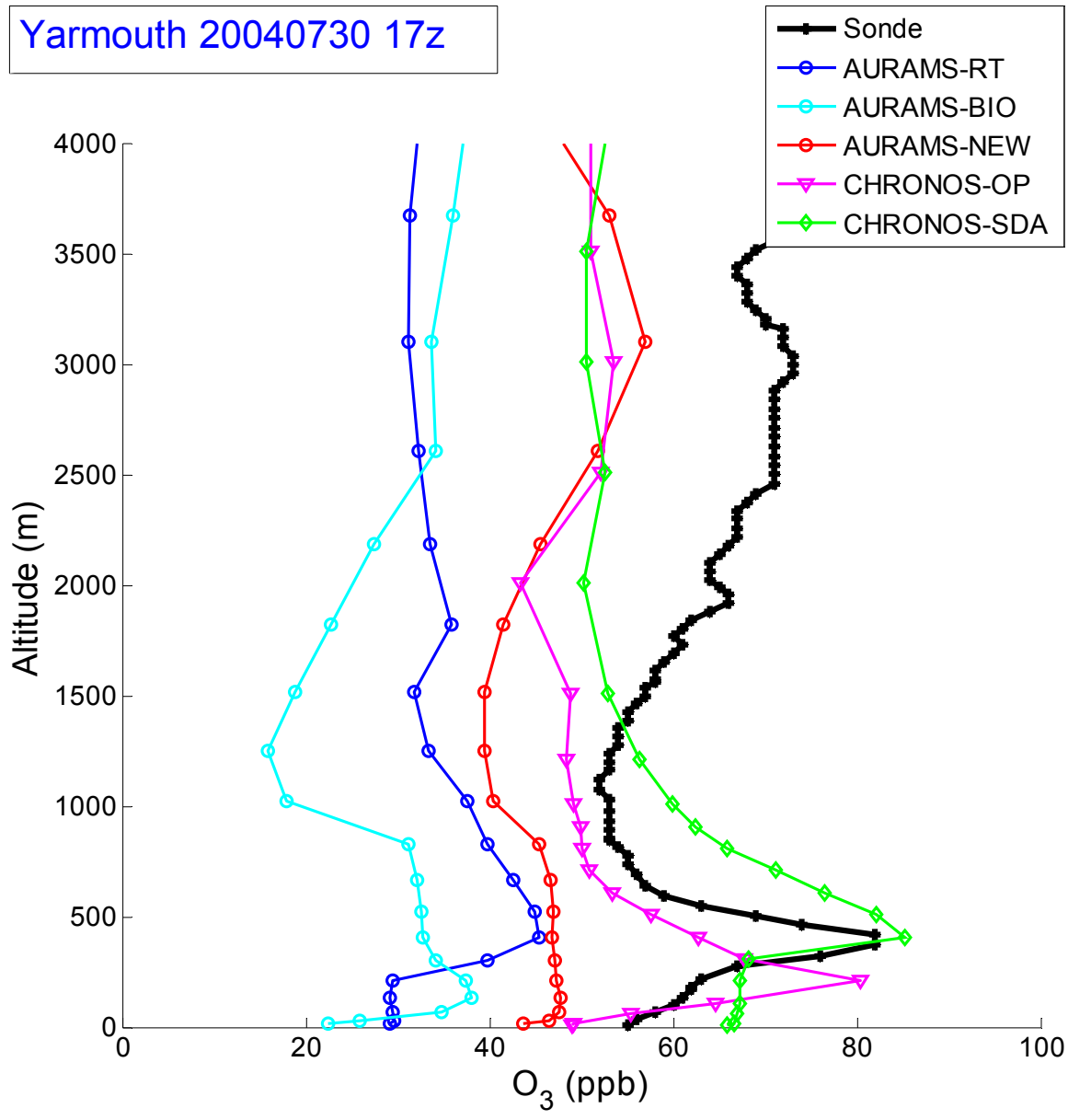

1

2 **Figure 4.** Ozone profile comparisons of the five model runs and the ozonesonde data, for July
3 30th at Yarmouth, Nova Scotia. What appears to be a marine boundary layer transition in the
4 vertical is surprisingly sharp for this late afternoon comparison. Nevertheless, the two
5 CHRONOS runs predict this well.

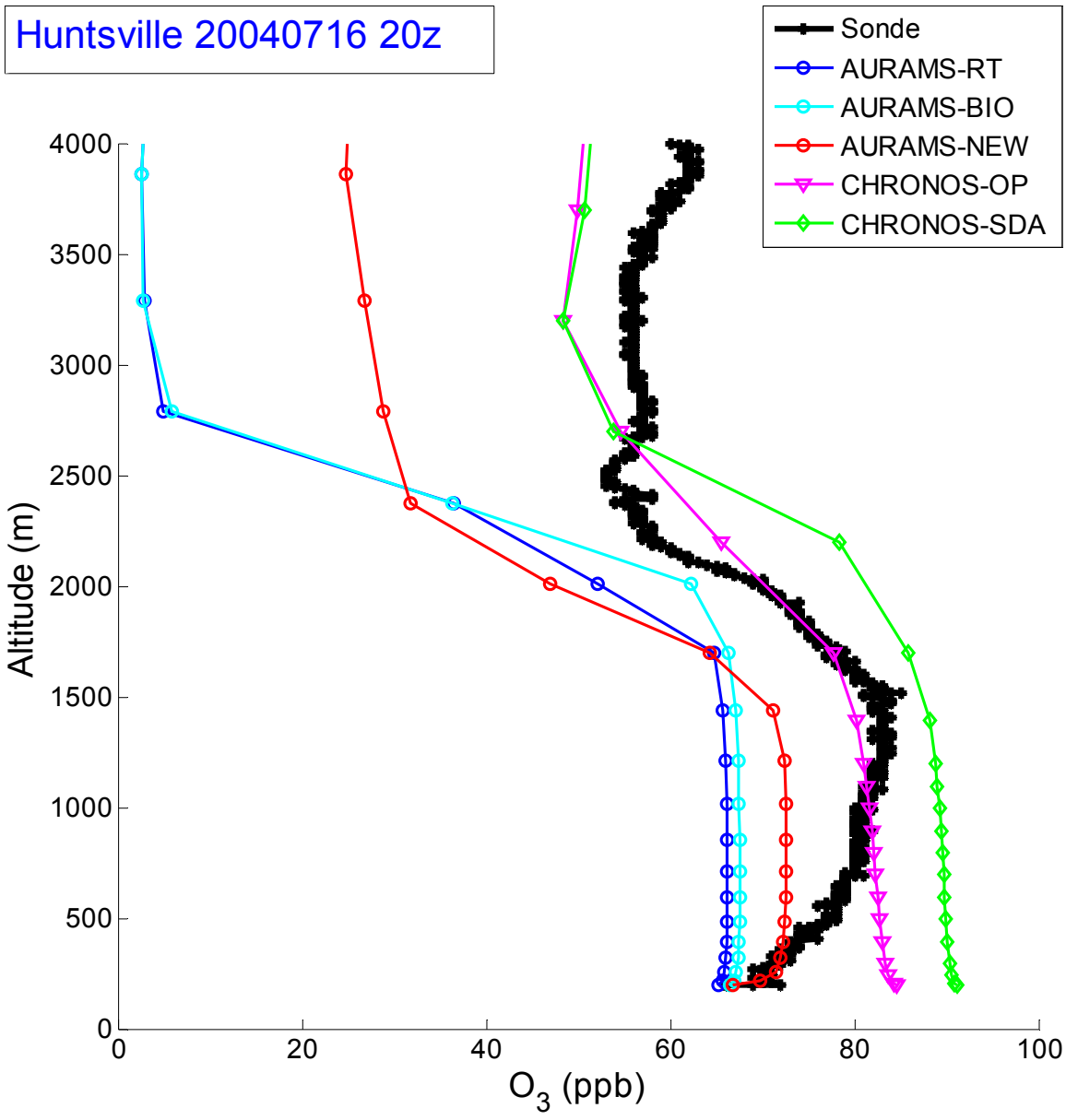

Figure 5. Ozone profile comparisons of the five model runs and the ozonesonde data, for July 16th at Huntsville, Alabama. All the models predict large ozone production in the surface layer, although underpredicting higher up.

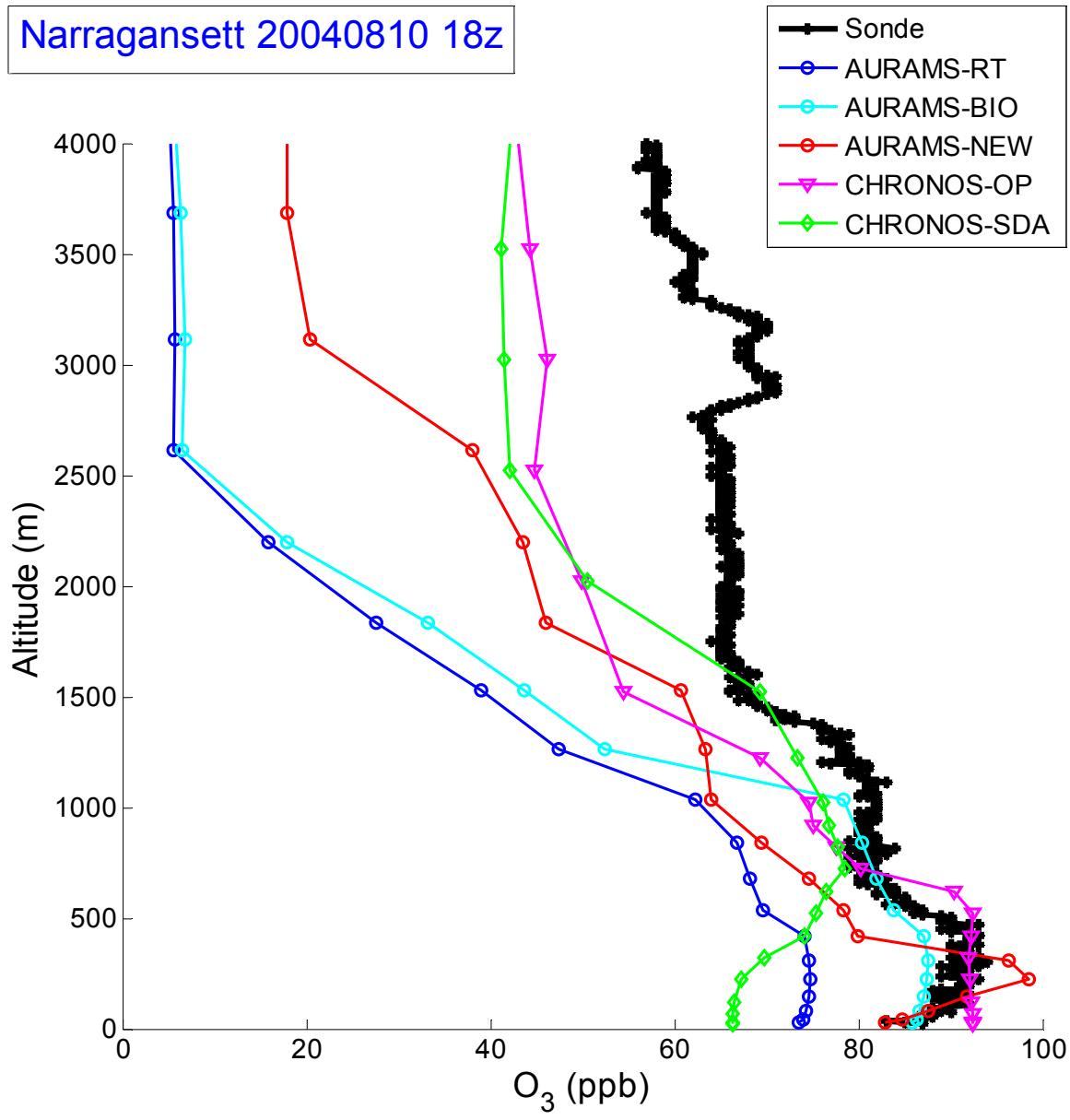

Figure 6. Ozone profile comparisons of the five model runs and the ozonesonde data, for August 10th at Narragansett, Rhode Island. All the models predict large ozone production in the surface layer, although underpredicting higher up. Some of the runs show some indication of the secondary peak at 1 km.

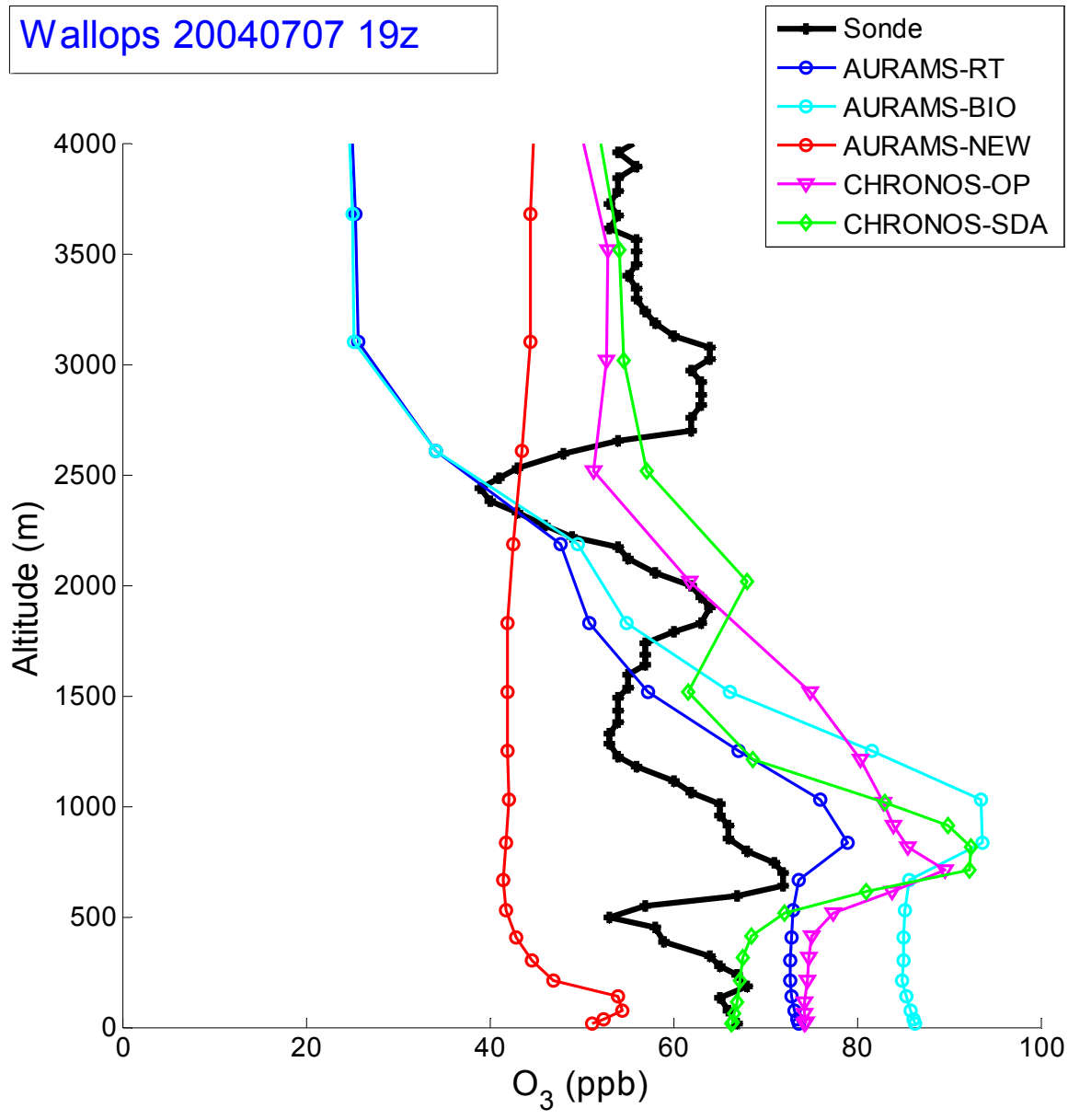

Figure 7. Ozone profile comparisons of the five model runs and the ozonesonde data, for July 7th at Wallops Island, Virginia. Four of the models predict the ozone feature near 1 km. Some of the runs show some indication of the secondary peak at 2 km.

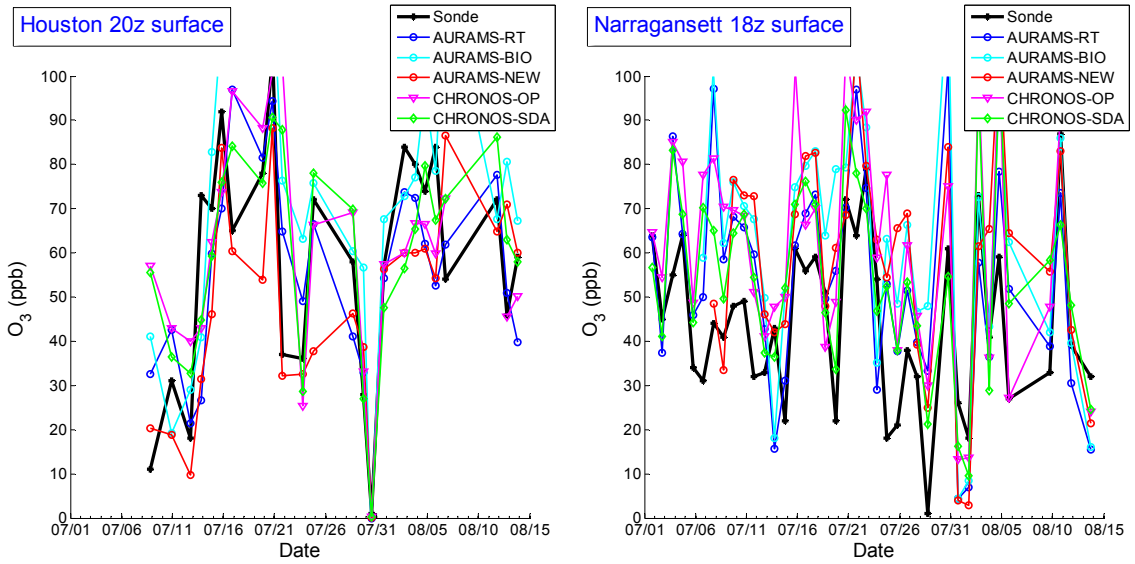
Houston 20z surface
Narragansett 18z surface
Sonde
AURAMS-RT
AURAMS-BIO
AURAMS-NEW
CHRONOS-OP
CHRONOS-SDA
O3 (ppb)
Date
07/01 07/06 07/11 07/16 07/21 07/26 07/31 08/05 08/10 08/15

1

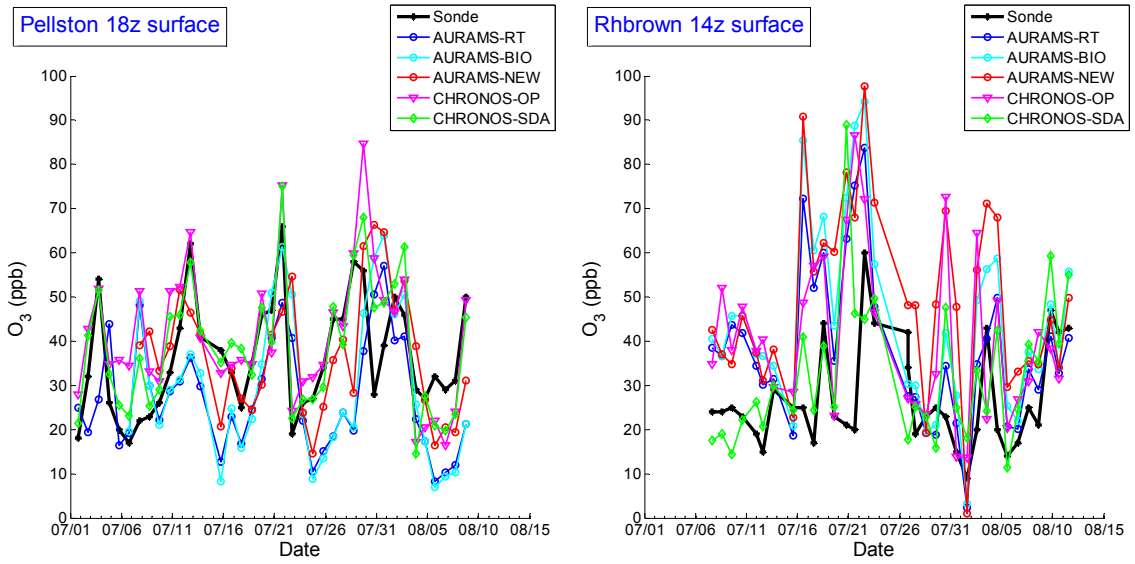
Pellston 18z surface
Rhbrown 14z surface
Sonde
AURAMS-RT
AURAMS-BIO
AURAMS-NEW
CHRONOS-OP
CHRONOS-SDA
O3 (ppb)
Date
07/01 07/06 07/11 07/16 07/21 07/26 07/31 08/05 08/10 08/15

2

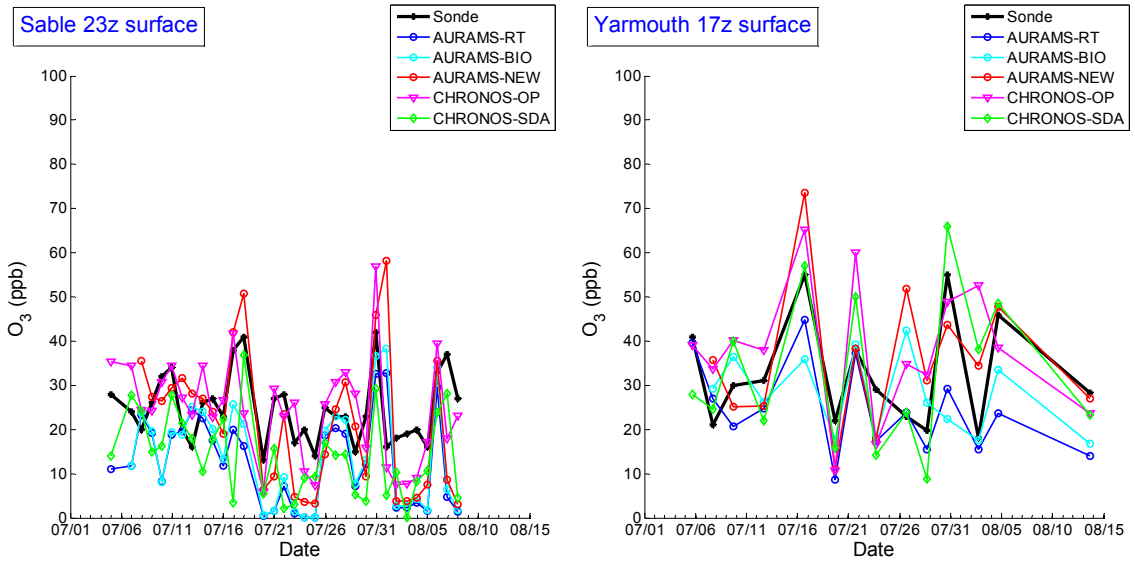
Sable 23z surface
Yarmouth 17z surface
Sonde
AURAMS-RT
AURAMS-BIO
AURAMS-NEW
CHRONOS-OP
CHRONOS-SDA
O3 (ppb)
Date
07/01 07/06 07/11 07/16 07/21 07/26 07/31 08/05 08/10 08/15

3

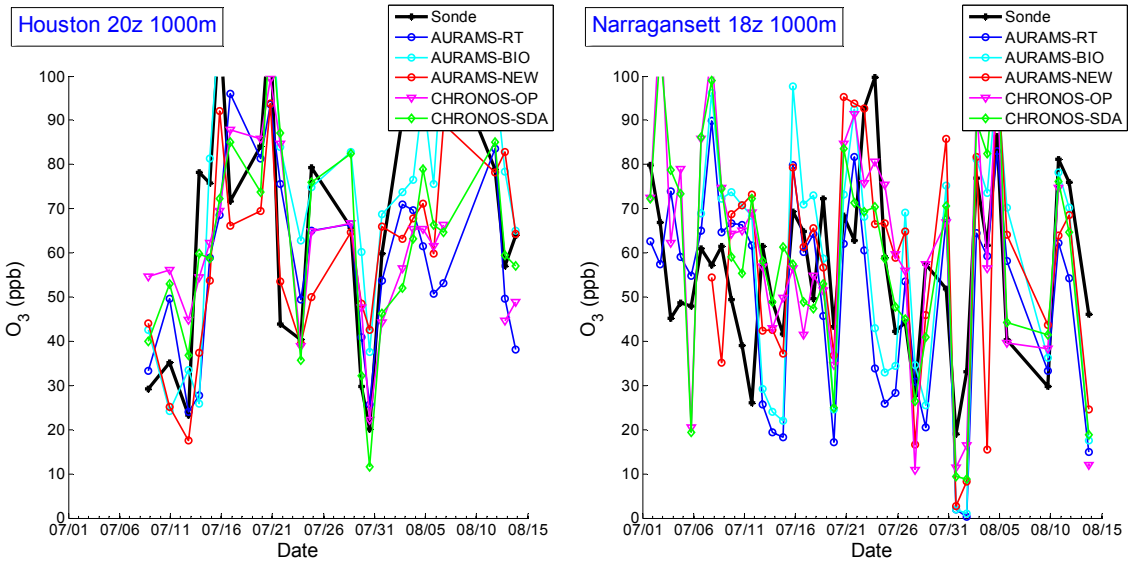
Houston 20z 1000m
Narragansett 18z 1000m
Sonde
AURAMS-RT
AURAMS-BIO
AURAMS-NEW
CHRONOS-OP
CHRONOS-SDA
O3 (ppb)
Date
07/01 07/06 07/11 07/16 07/21 07/26 07/31 08/05 08/10 08/15

1

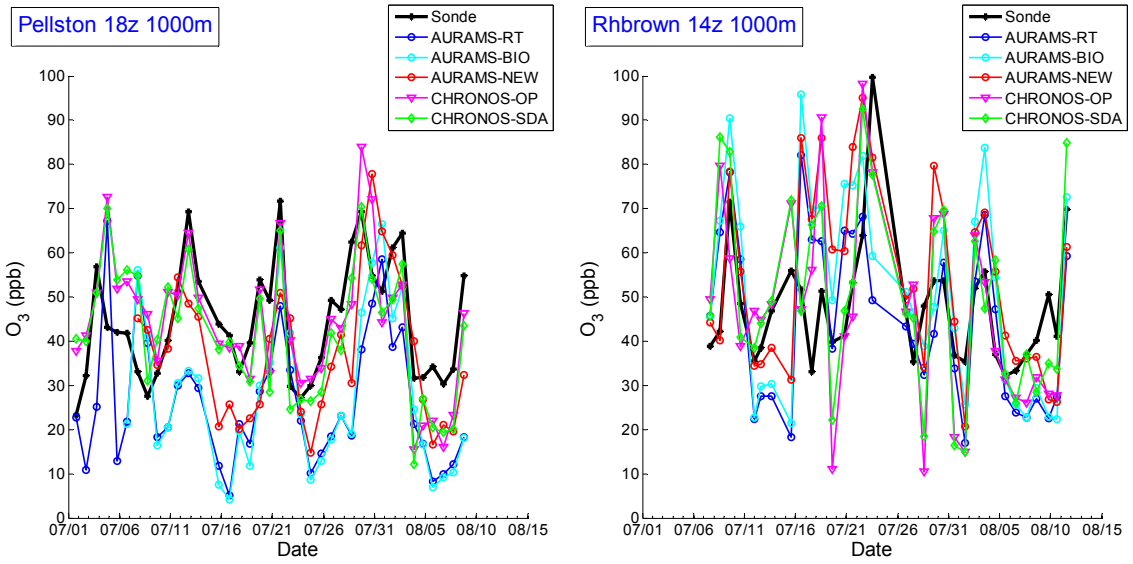
Pellston 18z 1000m
Rhbrown 14z 1000m
Sonde
AURAMS-RT
AURAMS-BIO
AURAMS-NEW
CHRONOS-OP
CHRONOS-SDA
O3 (ppb)
Date
07/01 07/06 07/11 07/16 07/21 07/26 07/31 08/05 08/10 08/15

2

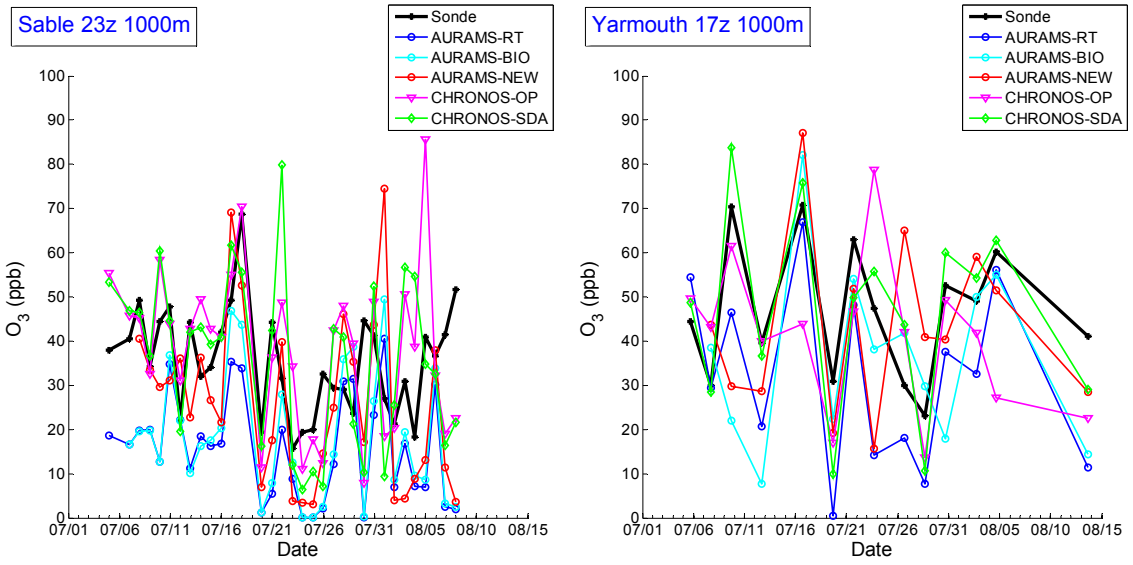
Sable 23z 1000m
Yarmouth 17z 1000m
Sonde
AURAMS-RT
AURAMS-BIO
AURAMS-NEW
CHRONOS-OP
CHRONOS-SDA
O3 (ppb)
Date
07/01 07/06 07/11 07/16 07/21 07/26 07/31 08/05 08/10 08/15

3

Figure 8. Surface ozone from ozonesondes at six IONS sites compared with the five model runs. Although individual differences are often significant, all the models track major changes in ozone concentration well. Variability in the model values is somewhat higher than in the measured values, by 12% , 32%, 38%, 27% and 17%, for AURAMS-RT, AURAMS-BIO, AURAMS-NEW, CHRONOS-OP and CHRONOS-SDA respectively.

Figure 9. Ozone at 1000m from the five model runs and the ozonesonde data, at six IONS sites. Although individual differences are often significant, all the models track major changes in ozone concentration well. Variability in the model values is somewhat higher than in the measured values, by 13%, 34%, 27%, 23%, and 29%, for AURAMS-RT, AURAMS-BIO, AURAMS-NEW, CHRONOS-OP and CHRONOS-SDA, respectively.

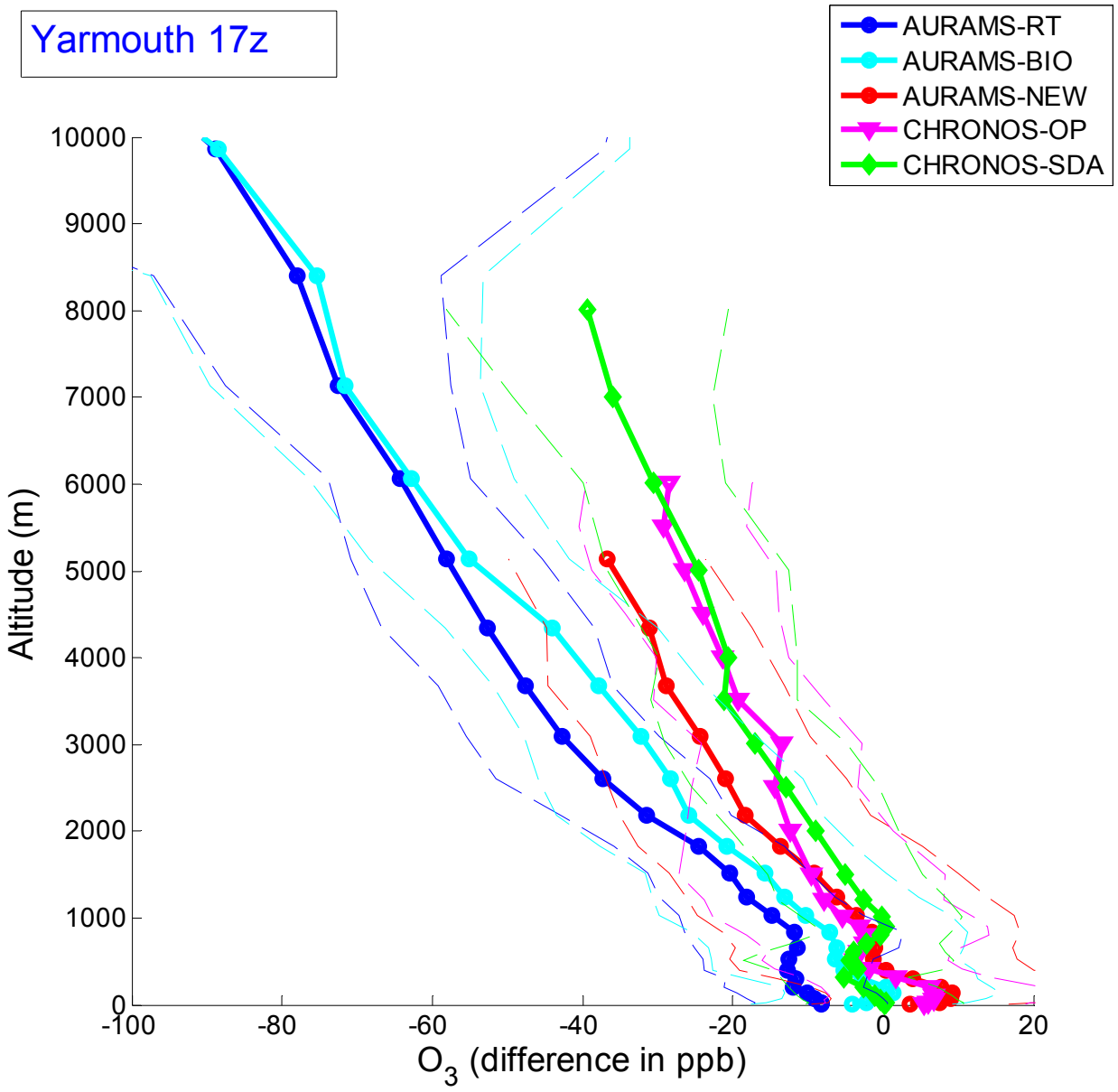

Figure 10. Average differences (model-sonde) between the observed and forecast ozone profiles for each model at Yarmouth, Nova Scotia. Dashed lines indicate 1σ limits. Differences for other sites are similar in the upper troposphere.

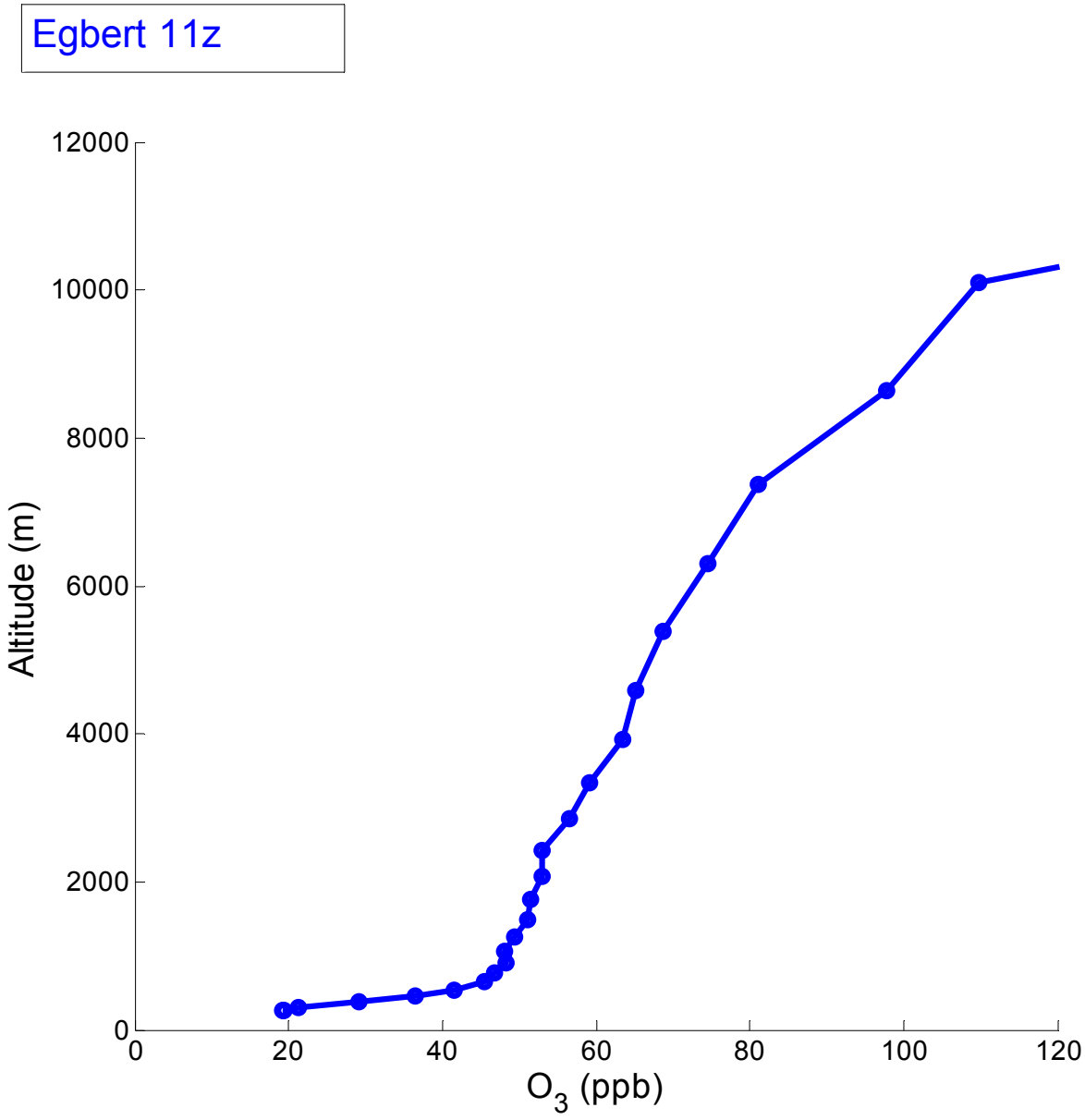

Figure 11. Ozone molar mixing ratio from ozonesondes at Egbert, Ontario, averaged on AURAMS model levels. As for other sites, ozone decreases monotonically from the stratosphere to the surface boundary layer.

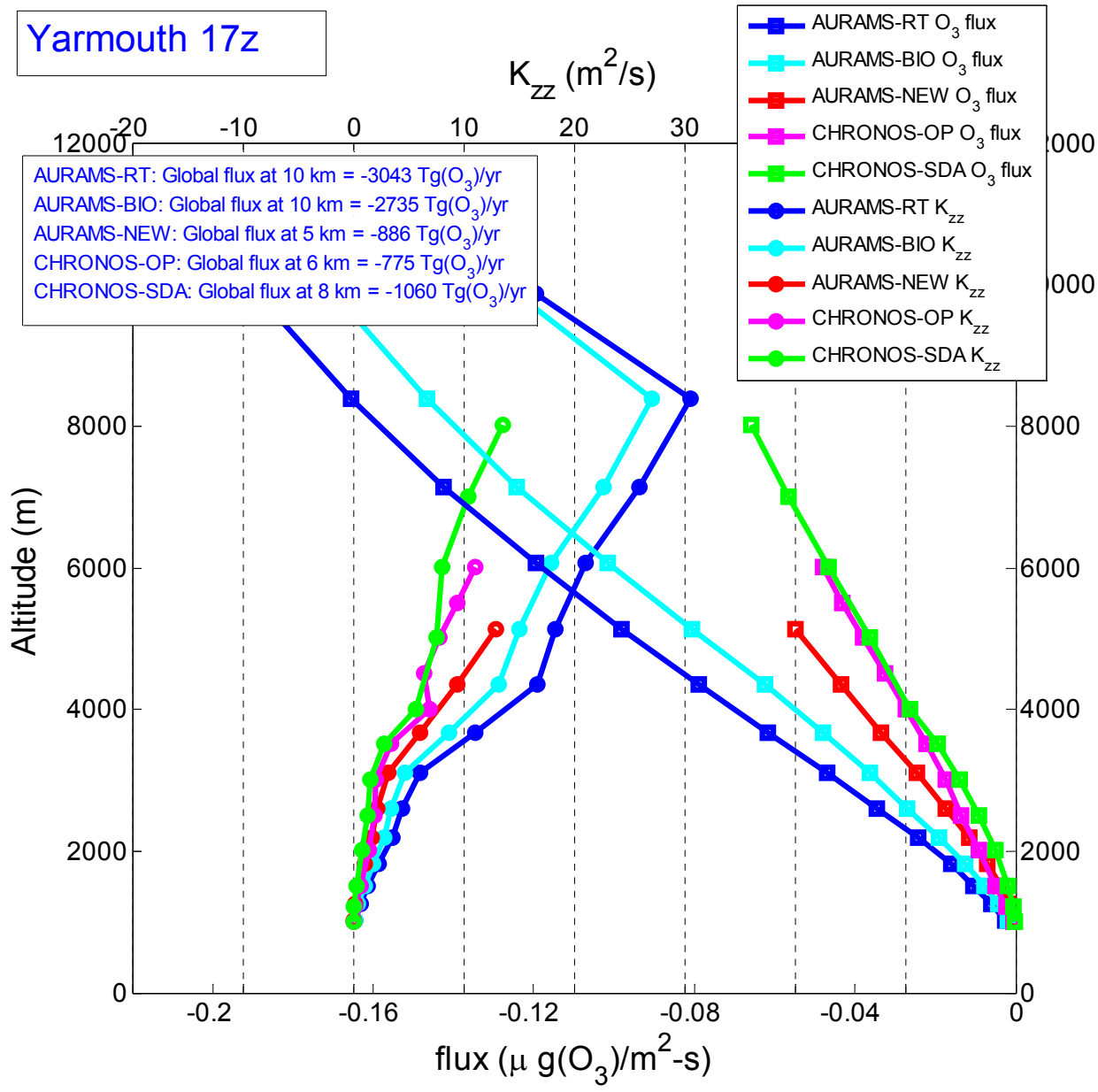

1

2 **Figure 12.** Calculated values of K_{zz} and cross-tropopause flux necessary to account for the
3 average differences between the observed and forecast ozone profiles shown in Figure 10.
4 Neither AURAMS nor CHRONOS includes a realistic stratosphere (although the AURAMS
5 model lid was set at 29 km for some of the ICARTT runs, the model did not include stratospheric
6 chemistry or any other source of large ozone mixing ratios in this region).